NASA TECHNICAL NOTE

NASA TN D-2187

NASA TN D-2187

RADIATION FROM SLOTTED-CYLINDER ANTENNAS IN A REENTRY PLASMA ENVIRONMENT

by Calvin T. Swift

Langley Research Center
Langley Station, Hampton, Va.

NATIONAL AERONAUTICS AND SPACE ADMINISTRATION • WASHINGTON, D. C. • FEBRUARY 1964

RADIATION FROM SLOTTED-CYLINDER ANTENNAS IN A REENTRY PLASMA ENVIRONMENT

By Calvin T. Swift

Langley Research Center
Langley Station, Hampton, Va.

NATIONAL AERONAUTICS AND SPACE ADMINISTRATION

For sale by the Office of Technical Services, Department of Commerce,
Washington, D.C. 20230 -- Price $1.75

CONTENTS

RADIATION FROM SLOTTED-CYLINDER ANTENNAS IN A REENTRY PLASMA ENVIRONMENT

By Calvin T. Swift

SUMMARY

A method is presented for calculating the equatorial patterns of slot antennas on conducting cylinders coated with plasmas which are inhomogeneous in a direction radially outward from the cylinder. The procedure consists of separating the wave equation into real and imaginary parts and numerically integrating between appropriate boundary conditions. The solutions are coefficients of the Fourier series which express the nature of the far-field pattern. The results differ from those obtained by plane-wave theory and demonstrate the desirability of this approach to predict signal attenuation of antennas in a radially varying plasma environment. Appendixes are included which outline procedures for solution of problems involving scattering, antenna arrays, and an aspect of the near-field problem.

Author

INTRODUCTION

When a hypersonic vehicle enters an atmosphere, a hot gas region is formed between the body and the shock wave; thereby, free electrons are generated to interact with electromagnetic radiation emitted from onboard antennas. If the ionization is sufficiently strong, a radio blackout condition may occur which disrupts communications over a large portion of the trajectory.

The electron density and collision frequency of the plasma, determined by appropriate flow-field analysis, are two important quantities needed to specify the complex index of refraction and, hence, the nature of the interaction. In general, at any given trajectory point, the electron concentration shows considerable variation, particularly in the direction normal to the vehicle; consequently, the propagation equations must be modified to include gradients of the index of refraction.

The radiation-source geometry is another important parameter. Considerable attention has been concentrated on two models - namely, the slot on the flat ground plane (refs. 1, 2, and 3) and the slot on the cylinder. The former has application to reentry problems provided the curvature of the body is neglected. This theory has been developed to include losses, finite plasma dimensions, anisotropic effects and finite-aperture size; however, inhomogeneous plasmas are excluded. If the wavelength is comparable to the vehicle size, the curvature of

the structure and surrounding plasma must be considered. To simplify the problem, a cylinder is selected as a reasonable mathematical model since this shape represents the aft portions of many reentry vehicles. The source configuration relevant to this geometry is the finite slot. The finite-slot representation of the physical picture, however, involves complicated mathematical procedures which restrict complete pattern calculations to plasma coatings that are homogeneous and nonlossy (refs. 4, 5, and 6). If the antenna is infinitely long, the geometry reduces to two dimensions and involves only the radial and azimuthal coordinates. The problem of the homogeneous lossy plasma has been solved in a recent report where collisions are included through the use of thin coating and high and low frequency approximations (ref. 7). The equations pertinent to the two-dimensional model can be extended to define interactions with inhomogeneous plasmas. However, the practical solutions of these equations, in general, are not specifiable because the plasma properties may vary arbitrarily within the shock layer. Therefore, analytical solutions (ref. 8) or WKB approximations are not realistic for many problems of interest and must be abandoned in favor of exact numerical techniques.

One numerical approach considers the plasma as a multilayered series of lossy homogeneous slabs (ref. 9). This technique has been derived for convenient application to plane waves at normal incidence to a plasma slab; however, this procedure may be inadequate to describe the present problem. The boundary conditions must be applied a large number of times and calculation of Bessel functions of complex arguments is required at each boundary. Since this approach seems to introduce computational difficulties, the alternative scheme of directly integrating the wave equation was chosen (refs. 10 and 11).

The mechanics of the scheme is as follows: First, all the fields are properly normalized so that the boundary conditions at the air-plasma interface are expressible in terms of the known quantities (Bessel functions, index of refraction, wave number, and the radial distance to the boundary). Second, all quantities are separated into real and imaginary parts. As a result, the number of boundary conditions at the air-plasma interface is doubled, and the wave equation expands into a pair of simultaneous second-order differential equations. Finally, the solutions of the wave equation and the excitation voltage at the conductor-plasma interface specify the unknown coefficients and, hence, the far-field pattern. Equatorial patterns for finite-slot antennas are also found from these solutions (ref. 4).

The primary topic of this paper is the single axial slot; however, appendixes A to E describe the necessary procedures which can be employed to calculate antenna patterns of circumferential slots, scattering patterns, antenna arrays, and the impedance of a cylindrical current.

SYMBOLS

$A_n, A_m, B_m, C_m, C_2, D_m$ coefficients

a_n, a_m, b_m, d_m, e_m

a radius of conducting cylinder, m

$a\phi_0$ width of slot, m

b radial extent of plasma coat, m

$\vec{E}$ electric field intensity, v/m

E_0 amplitude of plane wave, v/m

F_m radially dependent part of electric field intensity, v/m

G_m radially dependent part of magnetic field intensity, amp-turns/m

$\vec{H}$ magnetic field intensity, amp-turns/m

H_0 amplitude of plane wave, amp-turns/m

$H_m^{(2)}(k_0 r)$ Hankel function of second kind and of order m

J current density, amp/m^2

$J_m(k_0 r)$ Bessel function of order m

k wave number, m^{-1}

k_0 free-space wave number, m^{-1}

N_e electron density, m^{-3}

n index of refraction

$P(\phi)$ pattern factor

R source resistance per unit length, Ω/m

r, ϕ, z cylindrical coordinates

$\vec{u}_z$ unit vector in z-direction

V_0 applied potential on slot

$$V(r) = 1 - \frac{1}{\left[\frac{\omega}{\omega_p(r)}\right]^2 + \left[\frac{\nu(r)}{\omega_p(r)}\right]^2}$$

$$W(r) = \frac{\nu(r)/\omega_p(r)}{\omega/\omega_p(r)} \frac{1}{\left[\frac{\omega}{\omega_p(r)}\right]^2 + \left[\frac{\nu(r)}{\omega_p(r)}\right]^2}$$

X	source reactance per unit length, Ω/m
$Y_m(k_0 r)$	Neumann function of order m
x, y, z	Cartesian coordinates
Z	source impedance per unit length, Ω/m
Z_0	intrinsic impedance of free space, $\sqrt{\frac{\mu_0}{\epsilon_0}}$, 376.7 Ω
α	attenuation coefficient, nepers/m
δ	Dirac delta function
ϵ_0	permittivity of free space, 8.854×10^{-12} f/m
ϵ	permittivity, f/m
μ_0	permeability of free space, $4\pi \times 10^{-7}$ h/m
ν	electron collision frequency, collisions/sec
ϕ^*	dummy variable representing azimuthal coordinate of slot integration
ω	propagating frequency, radians/sec
ω_p	plasma frequency, $2\pi \times 8970 \times \sqrt{N_e}$ radians/sec

Subscripts:

spec	specified value
r, ϕ, z	vector components in principal directions

Superscripts:

0	dielectric region ($0 \leqq r \leqq a$)
I	plasma region
II	free-space region

i incident field component

s scattered field component

A prime denotes differentiation with respect to r.

ANALYSIS OF THE AXIAL SLOT

The model shown in figure 1 consists of an infinitely long conducting cylinder into which is cut a long radiating slot of finite width. The slot is excited by a tangentially applied electric field, uniformly distributed in the axial direction but specified across the slot. An exponential factor $e^{j\omega t}$ is chosen to describe the time dependence of the fields. The complex index of refraction of the plasma surrounding the cylinder is assumed to vary only in the radial direction.

The vector wave equation which describes the propagation of the magnetic vector in the presence of inhomogeneous media is of the form

$$\nabla^2\vec{H} + k_0^2 n^2 \vec{H} = -\frac{\vec{\nabla} n^2}{n^2} \times \left(\vec{\nabla} \times \vec{H}\right) \tag{1}$$

where the complex index of refraction n is a function of position. In general, equation (1) expands into three complicated differential equations. However, the restrictions imposed by the model generate certain simplifications.

The problem is two dimensional; thereby, the derivatives of the fields with respect to the z-coordinate vanish. Also,

$$E_z = H_r = H_\phi = 0 \tag{2}$$

Since the index of refraction varies only in the radial direction,

$$n = n(r) \tag{3}$$

and equation (1) reduces to

$$\frac{1}{r}\frac{\partial}{\partial r}\left[r \frac{\partial}{\partial r} H_z^I(r,\phi)\right] + \frac{1}{r^2}\frac{\partial^2}{\partial \phi^2} H_z^I(r,\phi) - \frac{1}{n^2}\frac{\partial n^2(r)}{\partial r}\frac{\partial H_z^I(r,\phi)}{\partial r} + k_0^2 n^2(r) H_z^I(r,\phi) = 0$$

$$(a \leqq r \leqq b) \tag{4}$$

Representing $H_z^I(r,\phi)$ by the following complex Fourier series

$$H_z^{I}(r,\phi) = \sum_{m=-\infty}^{\infty} G_m(r)e^{jm\phi} \tag{5}$$

transforms equation (4) into the following total differential equation:

$$\frac{1}{r}\frac{d}{dr}\left(r\frac{d}{dr}G_m\right) - \frac{1}{n^2}\frac{dn^2}{dr}\frac{dG_m}{dr} + k_0^2\left[n^2 - \frac{m^2}{(k_0r)^2}\right]G_m = 0 \qquad (a \leqq r \leqq b) \tag{6}$$

In order to properly satisfy the boundary conditions at $r = b$ it is necessary to know the functional behavior of the wave in free space. Since the index of refraction is constant in free space the solution is

$$H_z^{II}(r,\phi) = \sum_{m=-\infty}^{\infty} C_m H_m^{(2)}(k_0r)e^{jm\phi} \qquad (r \geqq b) \tag{7}$$

where $H_m^{(2)}(k_0r)$ is the Hankel function describing outgoing waves, and the coefficients C_m are to be determined.

The ϕ-components of the electric vector are also of interest. From the relationship

$$\vec{E} = \frac{1}{j\omega\epsilon}\vec{\nabla} \times \vec{H} \tag{8}$$

the respective E_ϕ-components in the plasma and in free space are given by

$$E_\phi^{I} = -\frac{1}{j\omega\epsilon(r)}\sum_{m=-\infty}^{\infty} G_m'(r)e^{jm\phi} \tag{9}$$

and

$$E_\phi^{II} = -\frac{1}{j\omega\epsilon_0}\sum_{m=-\infty}^{\infty} C_m H_m^{(2)'}(k_0r)e^{jm\phi} \tag{10}$$

Since the tangential components of the electric and magnetic fields must be continuous at $r = b$, the following boundary conditions must be satisfied:

$$\left.\begin{aligned} H_z^{I}(b,\phi) &= H_z^{II}(b,\phi) \\ E_\phi^{I}(b,\phi) &= E_\phi^{II}(b,\phi) \end{aligned}\right\} \tag{11a}$$

And, on the surface of the cylinder, $r = a$, the boundary conditions is given by

$$E_{\phi}^{I}(a,\phi) = E_{\phi,\,spec}(a,\phi) \tag{11b}$$

The specified electric field intensity $E_{\phi,\,spec}(a,\phi)$ can be expressed in terms of the Fourier expansion (ref. 12) as

$$E_{\phi,\,spec}(a,\phi) = \frac{1}{2\pi} \sum_{m=-\infty}^{\infty} e^{jm\phi} \int_{-\pi}^{\pi} E_{\phi}(a,\phi^*) e^{-jm\phi^*}\, d\phi^* \tag{12}$$

The applicability of the $E_{\phi,\,spec}$ term is qualified in appendix C.

By direct substitution, the boundary conditions (eqs. (11a) and (11b)) become at $r = b$

$$\left.\begin{aligned} C_m H_m^{(2)}(k_0 b) &= G_m(b) \\ C_m H_m^{(2)'}(k_0 b) &= \frac{\epsilon_0}{\epsilon(b)} G_m'(b) \end{aligned}\right\} \tag{13a}$$

and at $r = a$

$$-\frac{1}{j\omega\epsilon(a)} G_m'(a) = \frac{1}{2\pi} \int_{-\pi}^{\pi} E_{\phi}(a,\phi^*) e^{-jm\phi^*}\, d\phi^* \tag{13b}$$

These equations, for convenience, are normalized so that

$$\left.\begin{aligned} \frac{G_m(b)}{C_m} &= H_m^{(2)}(k_0 b) \\ \frac{G_m'(b)}{C_m} &= \frac{\epsilon(b)}{\epsilon_0} H_m^{(2)'}(k_0 b) \end{aligned}\right\} \tag{14a}$$

$$\frac{G_m'(a)}{C_m} = -\frac{j\omega\epsilon(a)}{2\pi C_m} \int_{-\pi}^{\pi} E_{\phi}(a,\phi^*) e^{-jm\phi^*}\, d\phi^* \tag{14b}$$

Having completed the normalization, it is convenient to separate the fields into real and imaginary parts by means of the definition

$$\frac{G_m(r)}{C_m} = t_m(r) + j u_m(r) \tag{15}$$

The real and imaginary parts of equations (14) can be separated to establish values of t_m, u_m, and their derivatives at $r = b$. As a result of this operation, the boundary conditions can be expressed in the following form:

$$t_m(b) = J_m(k_0 b) \tag{16}$$

$$u_m(b) = -Y_m(k_0 b) \tag{17}$$

$$t_m'(b) = V(b)\left[-k_0 J_{m+1}(k_0 b) + \frac{m}{b} J_m(k_0 b)\right] - W(b)\left[k_0 Y_{m+1}(k_0 b) - \frac{m}{b} Y_m(k_0 b)\right] \tag{18}$$

$$u_m'(b) = W(b)\left[-k_0 J_{m+1}(k_0 b) + \frac{m}{b} J_m(k_0 b)\right] + V(b)\left[k_0 Y_{m+1}(k_0 b) - \frac{m}{b} Y_m(k_0 b)\right] \tag{19}$$

where the dielectric constant has been separated into real and imaginary parts by means of the definition

$$\frac{\epsilon(r)}{\epsilon_0} = V(r) + jW(r) \tag{20}$$

Since the medium is a plasma, the expressions for $V(r)$ and $W(r)$ become

$$V(r) = 1 - \frac{1}{\left[\frac{\omega}{\omega_p(r)}\right]^2 + \left[\frac{\nu(r)}{\omega_p(r)}\right]^2} \tag{21}$$

and

$$W(r) = \frac{\nu(r)/\omega_p(r)}{\omega/\omega_p(r)} \frac{1}{\left[\frac{\omega}{\omega_p(r)}\right]^2 + \left[\frac{\nu(r)}{\omega_p(r)}\right]^2} \tag{22}$$

Because the index m assumes integer values, symmetry occurs in the boundary conditions so that

$$\left.\begin{aligned} t_{-m}(b) &= (-1)^m t_m(b) \\ u_{-m}(b) &= (-1)^m u_m(b) \\ t_{-m}'(b) &= (-1)^m t_m'(b) \\ u_{-m}'(b) &= (-1)^m u_m'(b) \end{aligned}\right\} \tag{23}$$

Other than a continuity requirement on the functions and their first derivatives, $V(r)$ and $W(r)$ may vary arbitrarily. Consequently, numerical integration of the wave equation is required. In order to properly initiate the integration, equation (6) is expressed in terms of t_m and u_m through equations (15) and (20). The left-hand side of equation (6) then separates into real and imaginary parts, each of which must independently vanish, and the result is the following set of simultaneous differential equations

$$\left.\begin{aligned}
&\frac{1}{r}\frac{d}{dr}\left(r\frac{dt_m}{dr}\right) - \frac{V}{V^2+W^2}\left(\frac{dV}{dr}\frac{dt_m}{dr} - \frac{dW}{dr}\frac{du_m}{dr}\right) - \frac{W}{V^2+W^2}\left(\frac{dW}{dr}\frac{dt_m}{dr} + \frac{dV}{dr}\frac{du_m}{dr}\right) + k_0^2\left\{\left[V - \frac{m^2}{(k_0r)^2}\right]t_m - Wu_m\right\} = 0 \\
&\frac{1}{r}\frac{d}{dr}\left(r\frac{du_m}{dr}\right) - \frac{V}{V^2+W^2}\left(\frac{dW}{dr}\frac{dt_m}{dr} + \frac{dV}{dr}\frac{du_m}{dr}\right) + \frac{W}{V^2+W^2}\left(\frac{dV}{dr}\frac{dt_m}{dr} - \frac{dW}{dr}\frac{du_m}{dr}\right) + k_0^2\left\{\left[V - \frac{m^2}{(k_0r)^2}\right]u_m + Wt_m\right\} = 0
\end{aligned}\right\} \quad (24)$$

Only positive values of m need be considered because of the recurrence relationship (eqs. (23)).

The solutions at $r = a$ and the boundary condition at $r = a$ (eqs. (14b) and (15)) determine the unknown coefficients C_m so that

$$C_m = -\frac{j\omega\epsilon(a)}{2\pi}\int_{-\pi}^{\pi} E_\phi(a,\phi^*)e^{-jm\phi^*}\,d\phi^*\left\{\frac{t_m'(a) - ju_m'(a)}{\left[t_m'(a)\right]^2 + \left[u_m'(a)\right]^2}\right\} \quad (25)$$

By substituting equation (25) into equation (7), and asymptotically expanding the Hankel function, the far-field value of $H_z^{II}(r,\phi)$ becomes

$$H_z^{II}(r,\phi) \approx \frac{\omega\epsilon(a)}{2\pi j}\sqrt{\frac{2}{\pi k_0 r}}\,e^{-j\left(k_0r - \frac{\pi}{4}\right)}\sum_{m=-\infty}^{\infty}\left\{\frac{t_m'(a) - ju_m'(a)}{\left[t_m'(a)\right]^2 + \left[u_m'(a)\right]^2}\right\}e^{jm\left(\phi+\frac{\pi}{2}\right)}\int_{-\pi}^{\pi} E_\phi(a,\phi^*)e^{-jm\phi^*}\,d\phi^* \quad (26)$$

The following equation for the far-field pattern is obtained by normalizing the absolute value of equation (26) by dividing by $\frac{\omega\epsilon_0 V_0}{2\pi a k_0}\sqrt{\frac{2}{\pi k_0 r}}$:

$$\left|P_z(\phi)\right| = \frac{k\phi}{\left(\frac{V_0}{a}\right)}\left|\frac{\epsilon(a)}{\epsilon_0}\right|\left|\sum_{m=-\infty}^{\infty}\left\{\frac{t_m'(a) - ju_m'(a)}{\left[t_m'(a)\right]^2 + \left[u_m'(a)\right]^2}\right\}e^{jm\left(\phi+\frac{\pi}{2}\right)}\int_{-\pi}^{\pi} E_\phi(a,\phi^*)e^{-jm\phi^*}\,d\phi^*\right| \quad (27)$$

Thus, the antenna pattern of an infinite-slot antenna of finite width in the ϕ-direction is determined by solving m sets of the differential equations (24) and summing appropriately to achieve the desired convergence of equation (27). Furthermore, the equatorial pattern of finite length slots are also determined by using this method along with the proper normalization factors.

If the applied electric field is singular $\left(E_\phi(a,\phi^*) = \frac{V_0}{a}\,\delta(\phi^*)\right)$, the integral in equation (27) is equal to V_0/a. In this case, equation (27) can be expressed in the form

$$\left|P_z(\phi)\right| = k_0\sqrt{V^2(a) + W^2(a)}\left|\sum_{m=-\infty}^{\infty}\left\{\frac{t_m'(a) - ju_m'(a)}{\left[t_m'(a)\right]^2 + \left[u_m'(a)\right]^2}\right\}e^{jm\left(\phi+\frac{\pi}{2}\right)}\right| \qquad (28)$$

RESULTS

Numerical integration of the propagation equations was performed on an electronic data processing system by the Runge-Kutta method with an accuracy of 10^{-7} per integration. The radiator was assumed to be a line source with $E_{\phi,\text{spec}} = \frac{V_0}{a}\,\delta(\phi^*)$; thus, the Fourier integral in equation (27) is equal to V_0/a. The computation of $P_z(\phi)$ was made at 10° increments in the range $0^\circ \leqq \phi \leqq 90^\circ$ and at 5° increments for $90^\circ \leqq \phi \leqq 180^\circ$. Free-space patterns were calculated by requiring all input values of the electron density to vanish.

A free-space pattern was manually computed and the agreement between these calculations and the computer results was excellent. The results of hand calculations were also compared with the numerical results for a case where region I was a homogeneous nonlossy plasma. Again, the computational comparisons were good. As a final test, the program was checked against the analytical results of a $1/r$ electron density distribution given in figures 4 and 9 of reference 8. Although the magnitudes could not be compared, the shapes of the numerically determined patterns were identical with those of reference 8.

The Homogeneous Plasma

The homogeneous plasma case was analyzed for expediency in determining general pattern behavior as a function of the various parameters - that is, plasma frequency, collision frequency, plasma thickness, and cylinder size. The free-space patterns for cylinders with $k_0a = 0.52$, 1.43, and 0.13 are shown in figure 2. Five plasma frequencies $(\omega/\omega_p = 0.01,\ 0.03,\ 0.10,\ 0.30,$ and $1.0)$ and three collision frequencies $(\nu/\omega = 0.300,\ 0.045,$ and $0.020)$ were selected to represent

possible values encountered under flight conditions. The three plasma depths considered correspond to $b/a = 1.2$, 1.6, and 2.0.

The patterns as a function of these parameters are plotted in figures 3 to 8. All the patterns shown in these figures are normalized so that the pattern strength at $\phi = 0^\circ$ represents an actual attenuation (or gain). In other words, the scale of the pattern is such that 0 db represents the free-space pattern strength at $\phi = 0^\circ$.

The most striking patterns are those in which the plasma frequency ratio ω/ω_p is of the order of unity. These patterns are strongly dependent upon changes in geometry and collision frequency, and it is difficult to discuss general pattern trends other than that the behavior becomes more anomalous as the collision frequency increases. It is of particular interest to note that a significant amount of radiation can be directed toward the rear of the antenna. When the ratio ω/ω_p becomes significantly less than unity, the patterns become much more regularly behaved.

An interesting feature of these curves is the relatively small amount of pattern shift at constant plasma thickness, particularly with regard to the smaller cylinder. Another interesting result is the increased forward directionality as the plasma thickness is increased. These observations are consistent with the results of appendix E; that is, if the magnitude of V is large, the approximate pattern can be specified by computing the free-space pattern of a line source located on a metallic cylinder of radius b and multiplying by the attenuation factor $2e^{-\alpha(b-a)\sqrt{\frac{a}{b}}}$.

The free-space pattern values at $\phi = 0^\circ$

$$P_z(\phi = 0) = \left| k_0 \sum_{m=-\infty}^{\infty} \frac{e^{jm\frac{\pi}{2}}}{H_m^{(2)'}(k_0 a)} \right|$$

are plotted in figure 9 as a function of $k_0 a$. This curve is significant because the absolute attenuation is given by

$$\text{Attenuation} = 2e^{-\alpha(b-a)} \frac{\left| k_0 \sum_{m=-\infty}^{\infty} \frac{e^{jm\frac{\pi}{2}}}{H_m^{(2)'}(k_0 b)} \right|}{\left| k_0 \sum_{m=-\infty}^{\infty} \frac{e^{jm\frac{\pi}{2}}}{H_m^{(2)'}(k_0 a)} \right|} \sqrt{\frac{a}{b}}$$

where both sums can be inferred from figure 9.

The Inhomogeneous Plasma

As a practical example of the techniques employed for the inhomogeneous plasma, consider the electron density and collision frequency distribution shown in figure 10. The curve for N_e with a maximum between the shock and the vehicle represents the case of flow which includes a viscous boundary layer, and the curve for N_e which continually increases from the shock to the body corresponds to an inviscid shock layer. The patterns resulting from the two flow-field assumptions are plotted in figures 11 and 12. At $\phi = 0^\circ$, the pattern attenuation is approximately -1.5 db for the viscous boundary-layer profile, and approximately -5.5 db for the completely inviscid profile. It is of interest to compare these values with the transmission coefficients computed with the use of plane-wave theory. In reference 11, the viscous and inviscid values were, respectively, -18.1 db and -34.8 db for these same plasma distributions. It is therefore very significant to note that the change of wave interaction model from the plane-wave slab type to the line-source cylinder type resulted in a large change in transmitted signal strength for an identical plasma coating. The importance of choosing appropriate wave propagation models for signal attenuation problems is clearly indicated from this comparison.

There is a large discrepancy between plane-wave and cylindrical-wave results; however, it must be emphasized that the fields inside the cylinder were ignored. Consequently, the boundary conditions were only partially applied at the surface of the cylinder. (See eq. (11b).) Although the proper boundary conditions at the slot are difficult to apply, the interior fields of the cylinder must be considered in order to properly compare the plane-wave and cylindrical-wave results.

CONCLUSIONS

A method for calculating the equatorial patterns of slot antennas on conducting cylinders has been presented. For expediency in determining general pattern behavior as a function of the various parameters, the homogeneous plasma case was analyzed and the following conclusions are noted from examination of the results:

1. Extreme pattern irregularities occur in the critical region (the ratio of signal frequency to plasma frequency ω/ω_p approximately equal to 1) of a homogeneous plasma. The patterns appear to be sensitive to changes in geometry and collision frequency, and it is possible for much of the radiated energy to be directed behind the antenna.

2. If a thick homogeneous plasma is overdense, the patterns can be approximated by computing the free-space pattern of a source located on the surface of a metallic cylinder of radius b, and multiplying this pattern by $2e^{-\alpha(b-a)\sqrt{\frac{a}{b}}}$, where α is attenuation coefficient and a is radius of conducting cylinder.

3. For values of $\omega/\omega_p < 1$, improved signal transmission occurs with increasing collision frequency.

4. The pattern is attenuated with decreasing values of ω/ω_p and increasing thicknesses of the homogeneous plasma.

5. The amount of energy transmitted through a plasma may be much greater than that predicted by plane-wave theory.

Langley Research Center,
National Aeronautics and Space Administration,
Langley Station, Hampton, Va., November 4, 1963.

APPENDIX A

THE CIRCUMFERENTIAL SLOT

The geometry of the slot antenna problem is shown in figure 1; however, the excitation of the slot is changed so that

$$E_r = E_\phi = H_z = 0 \tag{A1}$$

In this case, the entire interaction is uniquely described by the field component E_z. The wave equation which describes the propagation of the electric vector is expressible in the form

$$\nabla^2\vec{E} + k_0^2 n^2 \vec{E} = -\vec{\nabla}\left(\frac{\vec{\nabla} n^2}{n^2} \cdot \vec{E}\right) \tag{A2}$$

But,

$$\vec{E}_z = E(r,\phi)\vec{u}_z \tag{A3}$$

and

$$n = n(r)$$

Therefore, equation (A2) reduces to

$$\frac{1}{r}\frac{\partial}{\partial r}\left[r\frac{\partial E_z{}^I(r,\phi)}{\partial r}\right] + \frac{1}{r^2}\frac{\partial^2 E_z{}^I(r,\phi)}{\partial \phi^2} + k_0{}^2 n^2(r) E_z{}^I(r,\phi) = 0 \quad (a \leqq r \leqq b) \tag{A4}$$

Contrary to equation (4), equation (A4) does not depend upon the gradient of the complex index of refraction.

The free-space solutions of E_z and H_ϕ are

$$E_z{}^{II}(r,\phi) = \sum_{m=-\infty}^{\infty} D_m H_m^{(2)}(k_0 r) e^{jm\phi} \tag{A5}$$

$$H_\phi{}^{II}(r,\phi) = \frac{1}{j\omega\mu_0}\sum_{m=-\infty}^{\infty} D_m H_m^{(2)'}(k_0 r) e^{jm\phi} \tag{A6}$$

And in the inhomogeneous medium the solutions become

$$E_z^I(r,\phi) = \sum_{m=-\infty}^{\infty} F_m(r)e^{jm\phi} \tag{A7}$$

$$H_\phi^I(r,\phi) = \frac{1}{j\omega\mu_0} \sum_{m=-\infty}^{\infty} F_m'(r)e^{jm\phi} \tag{A8}$$

At the surface of the cylinder, $r = a$, the equation for the specified electric field intensity can be rewritten in the form

$$E_{z,spec}(a,\phi) = \frac{1}{2\pi} \sum_{m=-\infty}^{\infty} e^{jm\phi} \int_{-\pi}^{\pi} E_z(a,\phi^*)e^{-jm\phi^*}\, d\phi^* \tag{A9}$$

The tangential components of the fields must be continuous at the air-plasma interface, and the electric field must be a specified value at $r = a$. Therefore, the boundary conditions can be stated in terms of the following equations:

$$\frac{F_m(b)}{D_m} = H_m^{(2)}(k_0 b) \tag{A10a}$$

$$\frac{F_m'(b)}{D_m} = H_m^{(2)'}(k_0 b) \tag{A10b}$$

$$\frac{F_m(a)}{D_m} = \frac{1}{2\pi D_m} \int_{-\pi}^{\pi} E_z(a,\phi^*)e^{-jm\phi^*}\, d\phi^* \tag{A10c}$$

It is desirable to separate the real and imaginary parts of all the quantities involved. To accomplish this, let

$$\frac{F_m(r)}{D_m} = q_m(r) + js_m(r) \tag{A11}$$

As a result of equation (A11), the expression (A4) expands into the following set of simultaneous differential equations:

$$\left.\begin{aligned} \frac{1}{r}\frac{d}{dr}\left(r\frac{dq_m}{dr}\right) + k_0^2\left\{\left[V - \frac{m^2}{(k_0 r)^2}\right]q_m - Ws_m\right\} = 0 \\ \frac{1}{r}\frac{d}{dr}\left(r\frac{ds_m}{dr}\right) + k_0^2\left\{\left[V - \frac{m^2}{(k_0 r)^2}\right]s_m + Wq_m\right\} = 0 \end{aligned}\right\} \tag{A12}$$

As in the case of the axial slot, equations (A12) are integrated subject to the boundary conditions

$$\left.\begin{aligned} q_m(b) &= J_m(k_0 b) \\ s_m(b) &= -Y_m(k_0 b) \\ q_m'(b) &= -k_0 J_{m+1}(k_0 b) + \frac{m}{b} J_m(k_0 b) \\ s_m'(b) &= k_0 Y_{m+1}(k_0 b) - \frac{m}{b} Y_m(k_0 b) \end{aligned}\right\} \qquad (A13)$$

at $r = b$.

The solutions at $r = a$, and the boundary condition at $r = a$ (eq. (A10c)) are sufficient to specify the pattern. Through the appropriate algebraic manipulation, the far-field value of the electric field is

$$E_z^{II} \approx \frac{1}{2\pi}\sqrt{\frac{2}{\pi k_0 r}}\, e^{-j\left(k_0 r - \frac{\pi}{4}\right)} \sum_{m=-\infty}^{\infty} \frac{\left[q_m(a) - j s_m(a)\right]}{\left[q_m(a)\right]^2 + \left[s_m(a)\right]^2}\, e^{jm\left(\phi + \frac{\pi}{2}\right)} \int_{-\pi}^{\pi} E(a,\phi^*) e^{-jm\phi^*}\, d\phi^* \qquad (A14)$$

APPENDIX B

ARRAY OF SLOT ANTENNAS ON THE CYLINDER

When the problem of the single slot radiator is solved, patterns of a slot array may be defined without further numerical integrations; that is, the pattern expression (eq. (27)) is valid for any number of slots on the surface of the cylinder provided that all the source excitations are included in the integral

$$\int_{-\pi}^{\pi} E_{\phi}(a,\phi^*)e^{-jm\phi^*}\,d\phi^* \tag{B1}$$

As an example, suppose N slots of infinitesimal width each of amplitude $\frac{V_0}{a}A_n$ and phase ψ_n are located at points ϕ_n on the surface of the cylinder. In this example, the field at $r = a$ can be expressed in the form

$$E_{\phi}(a,\phi^*) = \frac{V_0}{a}\left[\sum_{n=1}^{N} A_n e^{j\psi_n}\delta\left(\phi^* - \phi_n\right)\right] \tag{B2}$$

And, the integral (B1) becomes

$$\left.\begin{aligned}\int_{-\pi}^{\pi} E_{\phi}(a,\phi^*)e^{-jm\phi^*}\,d\phi^* &= \frac{V_0}{a}\sum_{n=1}^{N} A_n e^{j\psi_n}\int_{-\pi}^{\pi}\delta\left(\phi^* - \phi_n\right)e^{-jm\phi^*}\,d\phi^* \\ \int_{-\pi}^{\pi} E_{\phi}(a,\phi^*)e^{-jm\phi^*} &= \frac{V_0}{a}\sum_{n=1}^{N} A_n e^{j\left(\psi_n - m\phi_n\right)}\end{aligned}\right\} \tag{B3}$$

The pattern for an array of thin slot antennas is therefore defined by the series

$$\left|P_z(\phi)\right| = k_0\left|\frac{\epsilon(a)}{\epsilon_0}\right|\left|\sum_{m=-\infty}^{\infty}\sum_{n=1}^{N} A_n\left\{\frac{t_m'(a) - ju_m'(a)}{\left[t_m'(a)\right]^2 + \left[u_m'(a)\right]^2}\right\}e^{jm\left(\phi-\phi_n+\frac{\pi}{2}\right)+j\psi_n}\right| \tag{B4}$$

APPENDIX C

IMPEDANCE OF A CYLINDER OF CURRENTS

If the circumferential slot described in appendix A is fully open the fields are independent of the azimuthal coordinate ϕ, and the appropriate differential equations become:

$$\left.\begin{aligned} \frac{1}{r}\frac{d}{dr}\left(r\frac{dq}{dr}\right) + k_0^2\left(Vq - sW\right) &= 0 \\ \frac{1}{r}\frac{d}{dr}\left(r\frac{ds}{dr}\right) + k_0^2\left(Vs + qW\right) &= 0 \end{aligned}\right\} \tag{C1}$$

These equations are numerically integrated from $r = b$ and $r = a$, with initial conditions

$$\left.\begin{aligned} q(b) &= J_0\left(k_0 b\right) \\ s(b) &= -Y_0\left(k_0 b\right) \\ q'(b) &= -k_0 J_1\left(k_0 b\right) \\ s'(b) &= k_0 Y_1\left(k_0 b\right) \end{aligned}\right\} \tag{C2}$$

where

$$q(r) + js(r) = \frac{E_z{}^{I}(r)}{D_0} \tag{C3}$$

At $r = a$ the specified electric field is a constant such that

$$E_{z,spec} = E_0 \tag{C4}$$

Thus, the boundary condition at $r = a$ requires that

$$q(a) + js(a) = \frac{E_0}{D_0} \tag{C5}$$

and the far-field value of $E_z{}^{II}$ becomes:

$$E_z{}^{II} \approx \frac{E_0}{q(a) + js(a)}\sqrt{\frac{2}{\pi k_0 r}}\, e^{-j\left(k_0 r - \frac{\pi}{4}\right)} \tag{C6}$$

Dividing the magnitude of equation (C6) by $E_0\sqrt{\frac{2}{\pi k_0 r}}$ defines the pattern which is the circle

$$\left|P_z(\phi)\right| \approx \frac{1}{\sqrt{q^2(a) + s^2(a)}} \tag{C7}$$

This result, however, is not the general solution because the wave may also propagate in the region $r < a$. This is a point which was not considered in previous sections of this report because of the difficulty in applying the boundary conditions. (See the introduction of ref. 13.) Instead of requiring a specified field to exist $r = a$, the current concept discussed by Harrington in reference 14 is introduced in order to generalize the nature of the source and to simplify the expression defining the source impedance. The geometry of this problem is shown in figure 13.

The boundary conditions at $r = b$ (eqs. (C2)) and the differential equations (eqs. (C1)) apply to this problem, however, the boundary conditions at $r = a$ must be altered, so that

$$\left.\begin{aligned} E_z^{\,O}(a) &= E_z^{\,I}(a) = D_0\left[q(a) + js(a)\right] \\ H_\phi^{\,I}(a) - H_\phi^{\,O}(a) &= \frac{D_0}{j\omega\mu_0}\left[q'(a) + js'(a)\right] - H_\phi^{\,O}(a) = J_z \end{aligned}\right\} \tag{C8}$$

Since the fields must be finite at $r = 0$, the solutions of E and H for $r \leqq 0$ must be of the form

$$\left.\begin{aligned} E_z^{\,O}(r) &= C_2 J_0(kr) \\ H_\phi^{\,O}(r) &= \frac{C_2}{j\omega\mu_0} J_0'(kr) = \frac{-kC_2}{j\omega\mu_0} J_1(kr) \end{aligned}\right\} \tag{C9}$$

The boundary conditions at $r = a$ require that:

$$\left.\begin{aligned} D_0\left[q(a) + js(a)\right] - C_2 J_0(ka) &= 0 \\ D_0\left[q'(a) + js'(a)\right] + kC_2 J_1(ka) &= j\omega\mu_0 J_z \end{aligned}\right\} \tag{C10}$$

Therefore, the solutions of the unknown coefficients are

$$D_0 = \frac{j\omega\mu_0 J_z J_0(ka)}{kJ_1(ka)\left[q(a) + js(a)\right] + J_0(ka)\left[q'(a) + js'(a)\right]} \tag{C11}$$

and

$$C_2 = \frac{\left[q(a) + js(a)\right] j\omega\mu_0 J_z}{kJ_1(ka)\left[q(a) + js(a)\right] + J_0(ka)\left[q'(a) + js'(a)\right]} \tag{C12}$$

The far-field expression for the magnitude of the electric vector therefore becomes

$$E_z^{II} \approx \frac{j\omega\mu_0 J_z J_0(ka) e^{-j\left(k_0 r - \frac{\pi}{4}\right)}}{kJ_1(ka)\left[q(a) + js(a)\right] + J_0(ka)\left[q'(a) + js'(a)\right]} \sqrt{\frac{2}{\pi k_0 r}} \tag{C13}$$

Normalizing the absolute value of equation (C13) with respect to $\frac{\omega\mu_0 J_z}{k_0}\sqrt{\frac{2}{\pi k_0 r}}$ results in the following expression for the pattern:

$$\left|P_z(\phi)\right| = k_0 \left\{ \frac{1}{\left[k \frac{J_1(ka)}{J_0(ka)} q(a) + q'(a)\right]^2 + \left[k \frac{J_1(ka)}{J_0(ka)} s(a) + s'(a)\right]^2} \right\}^{1/2} \tag{C14}$$

The source impedance per unit length of the cylinder of currents, as given by Harrington (ref. 14, p. 228) is, in the notation of the present paper,

$$Z = - \frac{2\pi a J_z^* E_z\Big|_{r=a}}{(2\pi a)^2 \left|J_z\right|^2} \tag{C15}$$

where J_z^* is the complex conjugate of the surface current density. Since

$$\left(E_z\right)_{r=a} = \frac{\left[q(a) + js(a)\right] j\omega\mu_0 J_z J_0(ka)}{kJ_1(ka)\left[q(a) + js(a)\right] + J_0(ka)\left[q'(a) + js'(a)\right]} \tag{C16}$$

equation (C15) becomes

$$Z = -j \frac{k_0 Z_0}{2\pi a} \frac{\left[q(a) + js(a)\right] J_0(ka)}{kJ_1(ka)\left[q(a) + js(a)\right] + J_0(ka)\left[q'(a) + js'(a)\right]}$$

$$Z = \frac{\left|P_z(\phi)\right|^2 Z_0}{2\pi k_0 a}\left[s(a) - jq(a)\right]\left\{\left[k \frac{J_1(ka)}{J_0(ka)} q(a) + q'(a)\right] - j\left[k \frac{J_1(ka)}{J_0(ka)} s(a) + s'(a)\right]\right\} \qquad \text{(C17)}$$

Therefore,

$$R = \frac{\left|P_z(\phi)\right|^2 Z_0}{2\pi k_0 a}\left\{s(a)\left[k \frac{J_1(ka)}{J_0(ka)} q(a) + q'(a)\right] - q(a)\left[k \frac{J_1(ka)}{J_0(ka)} s(a) + s'(a)\right]\right\} \qquad \text{(C18)}$$

and

$$X = -\frac{\left|P_z(\phi)\right|^2 Z_0}{2\pi k_0 a}\left\{s(a)\left[k \frac{J_1(ka)}{J_0(ka)} s(a) + s'(a)\right] + q(a)\left[k \frac{J_1(ka)}{J_0(ka)} q(a) + q'(a)\right]\right\} \qquad \text{(C19)}$$

APPENDIX D

SCATTERING FROM PLASMA COATED CYLINDERS

The problem discussed in this appendix is concerned with expressions which can be used to compute the scattering patterns of plane waves interacting with a cylinder which is coated with an inhomogeneous plasma. In order to present a general solution, two polarizations of the incident plane wave must be considered - namely, the electric vector directed parallel to the Z-axis, and the electric vector perpendicular to the Z-axis.

Case 1: Electric Vector Polarized Along the Z-Axis

The exponential dependence of a plane-wave incident on the cylinder along the positive X-axis can be transformed into a series of cylindrical functions (ref. 14, p. 232) such that

$$E_z^{i} = E_0 e^{-jk_0 x} = E_0 \sum_{m=-\infty}^{\infty} j^{-m} J_m(k_0 r) e^{jm\phi} \tag{D1}$$

When the plane wave interacts with the coated cylinder, scattering occurs; therefore, the field in free space is the sum of the incident and scattered energy, that is

$$E_z^{II} = E_z^{i} + E_z^{s} \tag{D2}$$

Since the scattered energy consists of outgoing waves, the solution must be of the form

$$E_z^{s} = E_0 \sum_{m=-\infty}^{\infty} j^{-m} a_m H_m^{(2)}(k_0 r) e^{jm\phi} \tag{D3}$$

Therefore, equation (D2) becomes

$$E_z^{II} = E_0 \sum_{m=-\infty}^{\infty} j^{-m} \left[J_m(k_0 r) + a_m H_m^{(2)}(k_0 r) \right] e^{jm\phi}$$

$$= E_0 \sum_{m=-\infty}^{\infty} \left[J_m(k_0 r) + a_m H_m^{(2)}(k_0 r) \right] e^{jm\left(\phi - \frac{\pi}{2}\right)} \tag{D4}$$

Also,

$$H_{\phi}^{II} = \frac{E_0}{j\omega\mu_0} \sum_{m=-\infty}^{\infty} \left[J_m'(k_0 r) + a_m H_m^{(2)'}(k_0 r) \right] e^{jm\left(\phi - \frac{\pi}{2}\right)} \tag{D5}$$

The field solutions in the plasma are of the form

$$E_z^{I} = \sum_{m=-\infty}^{\infty} F_m(r) e^{jm\phi} \tag{D6}$$

and

$$H_{\phi}^{I} = \frac{1}{j\omega\mu_0} \sum_{m=-\infty}^{\infty} F_m'(r) e^{jm\phi} \tag{D7}$$

and the continuity relationships at $r = b$ require that

$$\left.\begin{aligned} F_m(b) &= E_0 \left[J_m(k_0 b) + a_m H_m^{(2)}(k_0 b) \right] e^{-jm\frac{\pi}{2}} \\ F_m'(b) &= E_0 \left[J_m'(k_0 b) + a_m H_m^{(2)'}(k_0 b) \right] e^{-jm\frac{\pi}{2}} \end{aligned}\right\} \tag{D8}$$

The boundary conditions at $r = a$ require that

$$\left.\begin{aligned} E_z^{I}(a,\phi) &= 0 \\ H_{\phi}^{I}(a,\phi) &= J_z(a,\phi) \end{aligned}\right\} \tag{D9}$$

where the current density may be expressed as a Fourier expansion

$$J_z(a,\phi) = \frac{1}{2\pi} \sum_{m=-\infty}^{\infty} e^{jm\phi} \int_{-\pi}^{\pi} J_z(a,\phi^*) e^{-jm\phi^*} \, d\phi^* \tag{D10}$$

With the use of equation (D10) the boundary conditions may be written as follows:

$$\left.\begin{aligned} F_m'(a) &= 0 \\ F_m'(a) &= \frac{j\omega\mu_0}{2\pi} \int_{-\pi}^{\pi} J_z(a,\phi^*) e^{-jm\phi^*} \, d\phi^* \equiv b_m \end{aligned}\right\} \tag{D11}$$

If $F_m(r)$ is redefined such that

$$\frac{F_m(r)}{b_m} = q_m(r) + js_m(r) \tag{D12}$$

then the differential equations which describe wave propagation in region II become

$$\left.\begin{aligned} \frac{1}{r}\frac{d}{dr}\left(r\frac{dq_m}{dr}\right) + k_0^2\left[\left(V - \frac{m^2}{k_0^2 r_0^2}\right)q_m - s_m W\right] &= 0 \\ \frac{1}{r}\frac{d}{dr}\left(r\frac{ds_m}{dr}\right) + k_0^2\left[\left(V - \frac{m^2}{k_0^2 r^2}\right)s_m + q_m W\right] &= 0 \end{aligned}\right\} \tag{D13}$$

However, in this case the integration must begin at $r = a$, subject to the initial conditions

$$\left.\begin{aligned} q_m(a) &= 0 \\ s_m(a) &= 0 \\ q_m'(a) &= 1 \\ s_m'(a) &= 0 \end{aligned}\right\} \tag{D14}$$

The boundary conditions at $r = b$ (eqs. (D8)) and the solutions of the differential equations at $r = b$ result in the two following simultaneous equations:

$$\left.\begin{aligned} \frac{E_0}{b_m}\left[J_m(k_0 b) + a_m H_m^{(2)}(k_0 b)\right]e^{-jm\frac{\pi}{2}} &= q_m(b) + js_m(b) \\ \frac{E_0}{b_m}\left[J_m'(k_0 b) + a_m H_m^{(2)'}(k_0 b)\right]e^{-jm\frac{\pi}{2}} &= q_m'(b) + js_m'(b) \end{aligned}\right\} \tag{D15}$$

and the two unknown coefficients become

$$a_m = \frac{J_m'(k_0 b)\left[q_m(b) + js_m(b)\right] - J_m(k_0 b)\left[q_m'(b) + js_m'(b)\right]}{H_m^{(2)}(k_0 b)\left[q_m'(b) + js_m'(b)\right] - H_m^{(2)'}(k_0 b)\left[q_m(b) + js_m(b)\right]} \tag{D16}$$

$$b_m = \frac{2jE_0 e^{-jm\frac{\pi}{2}}}{\pi b\left\{H_m^{(2)}(k_0b)\left[q_m'(b) + js_m'(b)\right] - H_m^{(2)'}(k_0b)\left[q_m(b) + js_m(b)\right]\right\}} \tag{D17}$$

where use has been made of the relationship

$$J_m(k_0b)H_m^{(2)'}(k_0b) - H_m^{(2)}(k_0b)J_m'(k_0b) = -\frac{2j}{\pi b} \tag{D18}$$

Therefore, the far-field expression for the scattered energy is

$$E_z^s \approx E_0\sqrt{\frac{2}{\pi k_0 r}}\, e^{-j\left(k_0r - \frac{\pi}{4}\right)}\sum_{m=-\infty}^{\infty}\frac{J_m'(k_0b)\left[q_m(b) + js_m(b)\right] - J_m(k_0b)\left[q_m'(b) + js_m'(b)\right]}{H_m^{(2)}(k_0b)\left[q_m'(b) + js_m'(b)\right] - H_m^{(2)'}(k_0b)\left[q_m(b) + js_m(b)\right]}\, e^{jm\phi} \tag{D19}$$

The scattered field pattern is the absolute value of equation (D19). From equations (D10) and (D11), the surface current density is

$$J_z(a,\phi) = \frac{2E_0}{\omega\mu_0\pi b}\sum_{m=-\infty}^{\infty}\frac{e^{jm\left(\phi - \frac{\pi}{2}\right)}}{H_m^{(2)}(k_0b)\left[q_m'(b) + js_m'(b)\right] - H_m^{(2)'}(k_0b)\left[q_m(b) + js_m(b)\right]} \tag{D20}$$

Case 2: Electric Vector Polarized in X-Y Plane

The development in this section is similar to the preceding one except it is easier to operate with the magnetic vector because it consists of a Z-component only. As before, the field in free space is

$$H_z^{II} = H_0\sum_{m=-\infty}^{\infty}\left[J_m(k_0r) + d_mH_m^{(2)}(k_0r)\right]e^{jm\left(\phi - \frac{\pi}{2}\right)} \tag{D21}$$

where the scattered energy is represented by the second term on the right-hand side of the equation. And

$$E_\phi^{II} = -\frac{H_0}{j\omega\epsilon_0}\sum_{m=-\infty}^{\infty}\left[J_m'(k_0r) + d_mH_m^{(2)'}(k_0r)\right]e^{jm\left(\phi - \frac{\pi}{2}\right)} \tag{D22}$$

In the plasma, the fields are of the form

$$\left.\begin{aligned} H_z^I &= \sum_{m=-\infty}^{\infty} G_m(r)e^{jm\phi} \\ E_\phi^I &= -\frac{1}{j\omega\epsilon}\sum_{m=-\infty}^{\infty} G_m'(r)e^{jm\phi} \end{aligned}\right\} \tag{D23}$$

The boundary conditions at $r = b$ are

$$\left.\begin{aligned} H_0\left[J_m(k_0b) + d_mH_m^{(2)}(k_0b)\right]e^{-jm\frac{\pi}{2}} &= G_m(b) \\ H_0\left[J_m'(k_0b) + d_mH_m^{(2)\prime}(k_0b)\right]e^{-jm\frac{\pi}{2}} &= \frac{\epsilon_0}{\epsilon(b)}G_m'(b) \end{aligned}\right\} \tag{D24}$$

and at $r = a$

$$\left.\begin{aligned} G_m' &= 0 \\ G_m &= \frac{-1}{2\pi}\int_{-\pi}^{\pi} J_\phi(a,\phi^*)e^{-jm\phi^*}\,d\phi^* = e_m \end{aligned}\right\} \tag{D25}$$

By defining

$$\frac{G_m(r)}{e_m} = t_m(r) + ju_m(r) \tag{D26}$$

equations (D24) are integrated with

$$\left.\begin{aligned} t_m(a) &= 1 \\ u_m(a) &= 0 \\ t_m'(a) &= 0 \\ u_m'(a) &= 0 \end{aligned}\right\} \tag{D27}$$

as initial conditions.

The solutions to the differential equations at $r = b$ and the boundary conditions at $r = b$ determine the unknown coefficients in the form

$$d_m = \frac{\left[V(b) + jW(b)\right]\left[t_m(b) + ju_m(b)\right]J_m'(k_0b) - J_m(k_0b)\left[t_m'(b) + ju_m'(b)\right]}{H_m^{(2)}(k_0b)\left[t_m'(b) + ju_m'(b)\right] - \left[t_m(b) + ju_m(b)\right]\left[V(b) + jW(b)\right]H_m^{(2)'}(k_0b)} \tag{D28}$$

$$e_m = \frac{2jH_0\left[V(b) + jW(b)\right]e^{-jm\frac{\pi}{2}}}{\pi b\left\{H_m^{(2)}(k_0b)\left[t_m'(b) + ju_m'(b)\right] - H_m^{(2)'}(k_0b)\left[V(b) + jW(b)\right]\left[t_m(b) + ju_m(b)\right]\right\}} \tag{D29}$$

The far-field expression for the scattered energy is of the form

$$H_z^s \approx H_0\sqrt{\frac{2}{\pi k_0 r}}\, e^{-j\left(k_0 r - \frac{\pi}{4}\right)}\sum_{m=-\infty}^{\infty}\frac{\left[V(b) + jW(b)\right]\left[t_m(b) + ju_m(b)\right]J_m'(k_0b) - \left[t_m'(b) + ju_m'(b)\right]J_m(k_0b)}{H_m^{(2)}(k_0b)\left[t_m'(b) + ju_m'(b)\right] - \left[t_m(b) + ju_m(b)\right]\left[V(b) + jW(b)\right]H_m^{(2)'}(k_0b)}\, e^{jm\phi} \tag{D30}$$

and the surface current density is

$$J_\phi(a,\phi) = \frac{2jH_0}{\pi b k_0}\left[V(b) + jW(b)\right]\sum_{m=-\infty}^{\infty}\frac{e^{jm\left(\phi - \frac{\pi}{2}\right)}}{\frac{H_m^{(2)'}(k_0b)}{k_0}\left[V(b) + jW(b)\right]\left[t_m(b) + ju_m(b)\right] - \frac{H_m^{(2)}(k_0b)}{k_0}\left[t_m'(b) + ju_m'(b)\right]} \tag{D31}$$

APPENDIX E

DETERMINATION OF APPROXIMATE PATTERNS

The equation which describes the propagation of electromagnetic waves radiating from an axial slot into a homogeneous plasma is of the form:

$$\frac{1}{r}\frac{d}{dr}\left(r\frac{dG_m}{dr}\right) + k_0^2\left[n^2 - \frac{m^2}{(k_0 r)^2}\right]G_m = 0 \tag{E1}$$

The solution to this equation can be expressed as a linear combination of Hankel functions, so that

$$G_m = A_m H_m^{(1)}(nk_0 r) + B_m H_m^{(2)}(nk_0 r) \tag{E2}$$

If the argument $nk_0 r$ is large, an asymptotic expansion results in the following solution

$$G_m \approx \frac{1}{\sqrt{nk_0 r}}\left(a_m e^{jnk_0 r} + b_m e^{-jnk_0 r}\right) \tag{E3}$$

And, the derivative of equation (E3) is

$$G_m' \approx \frac{j\sqrt{nk_0 r}}{r}\left(a_m e^{jnk_0 r} - b_m e^{-jnk_0 r}\right) \tag{E4}$$

The boundary conditions (eqs. (13a) and (13b)) result in the following equations for a line source radiating into the plasma

$$\left.\begin{aligned}
&\frac{a_m e^{jnk_0 b}}{\sqrt{nk_0 b}} + \frac{b_m e^{-jnk_0 b}}{\sqrt{nk_0 b}} - C_m H_m^{(2)}(k_0 b) = 0 \\
&\frac{a_m j}{n^2}\sqrt{\frac{nk_0}{b}}\, e^{jnk_0 b} - \frac{b_m j}{n^2}\sqrt{\frac{nk_0}{b}}\, e^{-jnk_0 b} - C_m H_m^{(2)'}(k_0 b) = 0 \\
&-\frac{a_m}{\omega\epsilon}\sqrt{\frac{nk_0}{a}}\, e^{jnk_0 a} + \frac{b_m}{\omega\epsilon}\sqrt{\frac{nk_0}{a}}\, e^{-jnk_0 a} = \frac{V_0}{2\pi a}
\end{aligned}\right\} \tag{E5}$$

A few algebraic manipulations result in a solution of the unknown coefficients in the form

$$C_m = -j \frac{V_0}{a} \frac{1}{2\pi} \frac{n\omega\epsilon_0}{k_0} \frac{\sqrt{a/b}}{H_m^{(2)}(k_0 b)\sin nk_0(b-a) + \frac{n}{k_0} H_m^{(2)'}(k_0 b)\cos nk_0(b-a)} \tag{E6}$$

But, because $\frac{n}{k_0} \gg 1$

$$C_m \approx -j \frac{V_0}{a} \frac{1}{2\pi} \omega\epsilon_0 \sqrt{\frac{a}{b}} \frac{1}{H_m^{(2)'}(k_0 b)\cos nk_0(b-a)} \tag{E7}$$

Consequently,

$$H_z^{II}(r,\phi) \approx -j \frac{V_0}{a} \frac{1}{2\pi} \omega\epsilon_0 \sqrt{\frac{a}{b}} \frac{e^{-j\left(k_0 r - \frac{\pi}{4}\right)}}{\cos nk_0(b-a)} \sum_{m=-\infty}^{\infty} \frac{e^{jm\left(\phi + \frac{\pi}{2}\right)}}{H_m^{(2)'}(k_0 b)} \tag{E8}$$

If the cylinder is uncoated, the solution to the problem is

$$H_z^{II}(r,\phi) \approx -j \frac{V_0}{a} \frac{1}{2\pi} \omega\epsilon_0 e^{-j\left(k_0 r - \frac{\pi}{4}\right)} \sum_{m=-\infty}^{\infty} \frac{e^{jm\left(\phi + \frac{\pi}{2}\right)}}{H_m^{(2)'}(k_0 b)} \tag{E9}$$

In view of the similarity of equations (E8) and (E9), the pattern of a coated cylinder, with the approximations given, can be expressed in the form

$$P_z(\phi) = \sqrt{\frac{a}{b}} \frac{1}{|\cos nk\,(b-a)|} P_z^*(\phi) \tag{E10}$$

where $P_z^*(\phi)$ is the free-space pattern of a source located on a perfectly conducting cylinder of radius b. Furthermore, if the plasma thickness is sufficiently large, equation (E10) becomes:

$$P_z(\phi) \approx 2e^{-\alpha(b-a)} \sqrt{\frac{a}{b}} P_z^*(\phi) \tag{E11}$$

REFERENCES

1. Hodara, H.: Radiation From a Gyro-Plasma Sheathed Aperture. IEEE Trans. on Antennas and Propagation, vol. AP-11, no. 1, Jan. 1963, pp. 2-12.

2. Tamir, T., and Oliner, A. A.: The Influence of Complex Waves on the Radiation Field of a Slot-Excited Plasma Layer. IRE Trans. on Antennas and Propagation, vol. AP-10, no. 1, Jan. 1962, pp. 55-65.

3. Omura, Masayuki: Radiation Pattern of a Slit in a Ground Plane Covered by a Plasma Layer. AFCRL-62-958, Office Aerospace Res., U.S. Air Force, Dec. 1962.

4. Knop, Charles M.: The Radiation Fields From a Circumferential Slot on a Metal Cylinder Coated With a Lossy Dielectric. IRE Trans. on Antennas and Propagation, vol. AP-9, no. 6, Nov. 1961, pp. 535-545.

5. Rusch, W. V. T.: Radiation From a Plasma-Clad Axially-Slotted Cylinder. USCEC Rep. 82-201 (AFCRL 714), Univ. of Southern California, May 1962.

6. Harris, J. H.: Radiation Through Cylindrical Plasma Sheaths. Sci. Rep. No. 2 (AFCRL-62-976), Hughes Aircraft Co., Aug. 1962.

7. Sengupta, Dipak L.: The Radiation Field Produced by an Infinite Slot in an Infinite Cylinder Surrounded by a Homogeneous Plasma Sheath. 4563-35-T (Contract AF 33(616)-8365), Inst. Sci. and Tech., Univ. of Michigan, May 1963.

8. Yeh, Cavour W. H., and Kaprielian, Z. A.: Radiation From an Axially Slotted Cylinder Coated With an Inhomogeneous Dielectric Sheath. USCEC Rep. 82-207 (AFCRL-62-963), Univ. of Southern California, Dec. 1962.

9. Harley, T. P., and Tyras, G.: Transmission of Electromagnetic Waves Through an Ionized Layer in the Presence of a Strong Magnetic Field. Proc. IRE, vol. 49, no. 12, Dec. 1961, pp. 1822-1824.

10. Richmond, J. H.: Transmission Through Inhomogeneous Plane Layers. IRE Trans. on Antennas and Propagation, vol. AP-10, no. 3, May 1962, pp. 300-305.

11. Swift, Calvin T., and Evans, John S.: Generalized Treatment of Plane Electromagnetic Waves Passing Through an Isotropic Inhomogeneous Plasma Slab at Arbitrary Angles of Incidence. NASA TR R-172, 1963.

12. Wait, James R.: Electromagnetic Radiation From Cylindrical Structures. Pergamon Press, 1959.

13. Silver, Samuel, and Saunders, William K.: The External Field Produced by a Slot in an Infinite Circular Cylinder. Jour. Appl. Phys., vol. 21, no. 2, Feb. 1950, pp. 153-158.

14. Harrington, Roger F.: Time-Harmonic Electromagnetic Fields. McGraw-Hill Book Co., Inc., 1961.

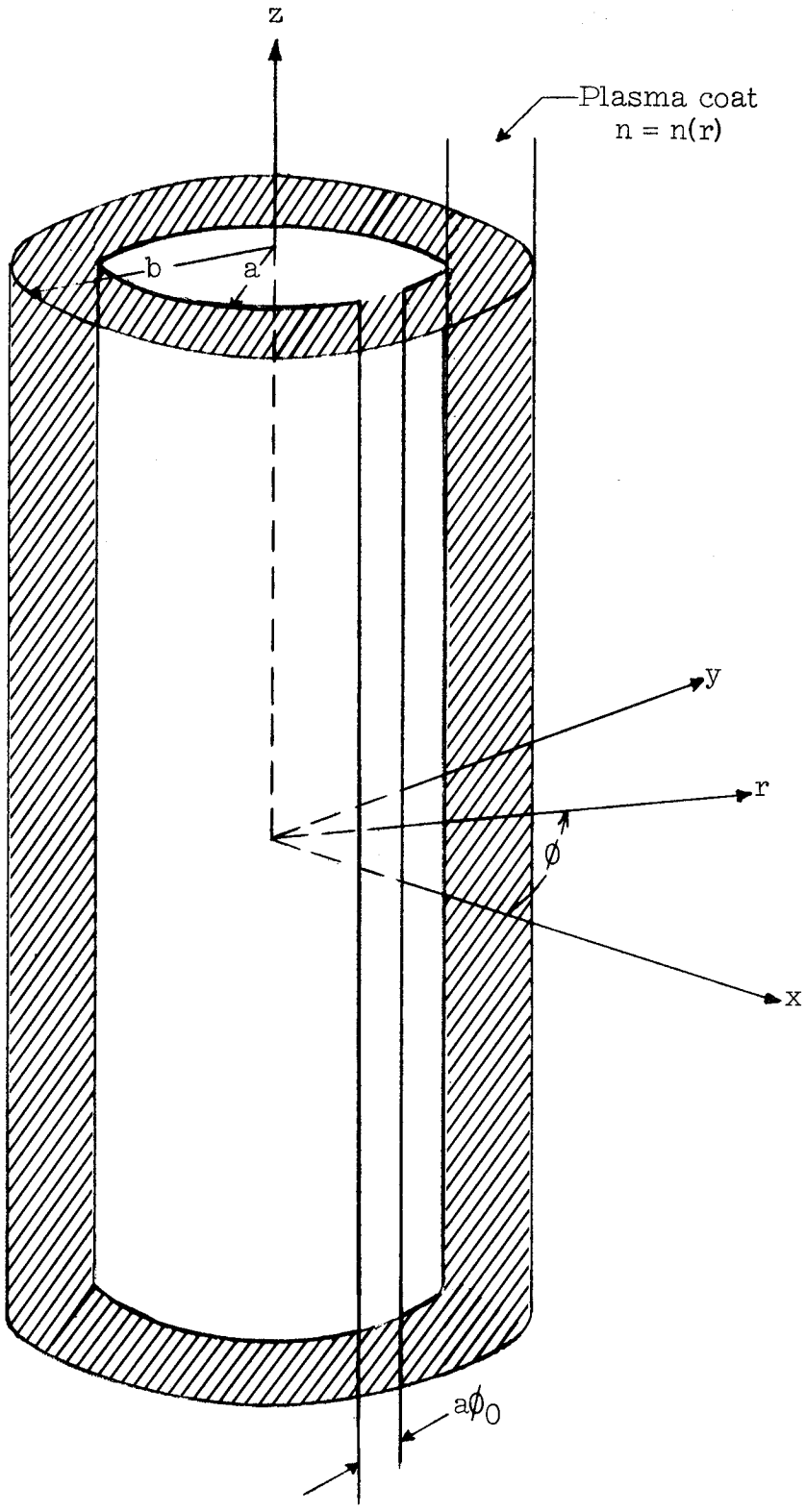

Figure 1.- Geometry of the slot antenna problem.

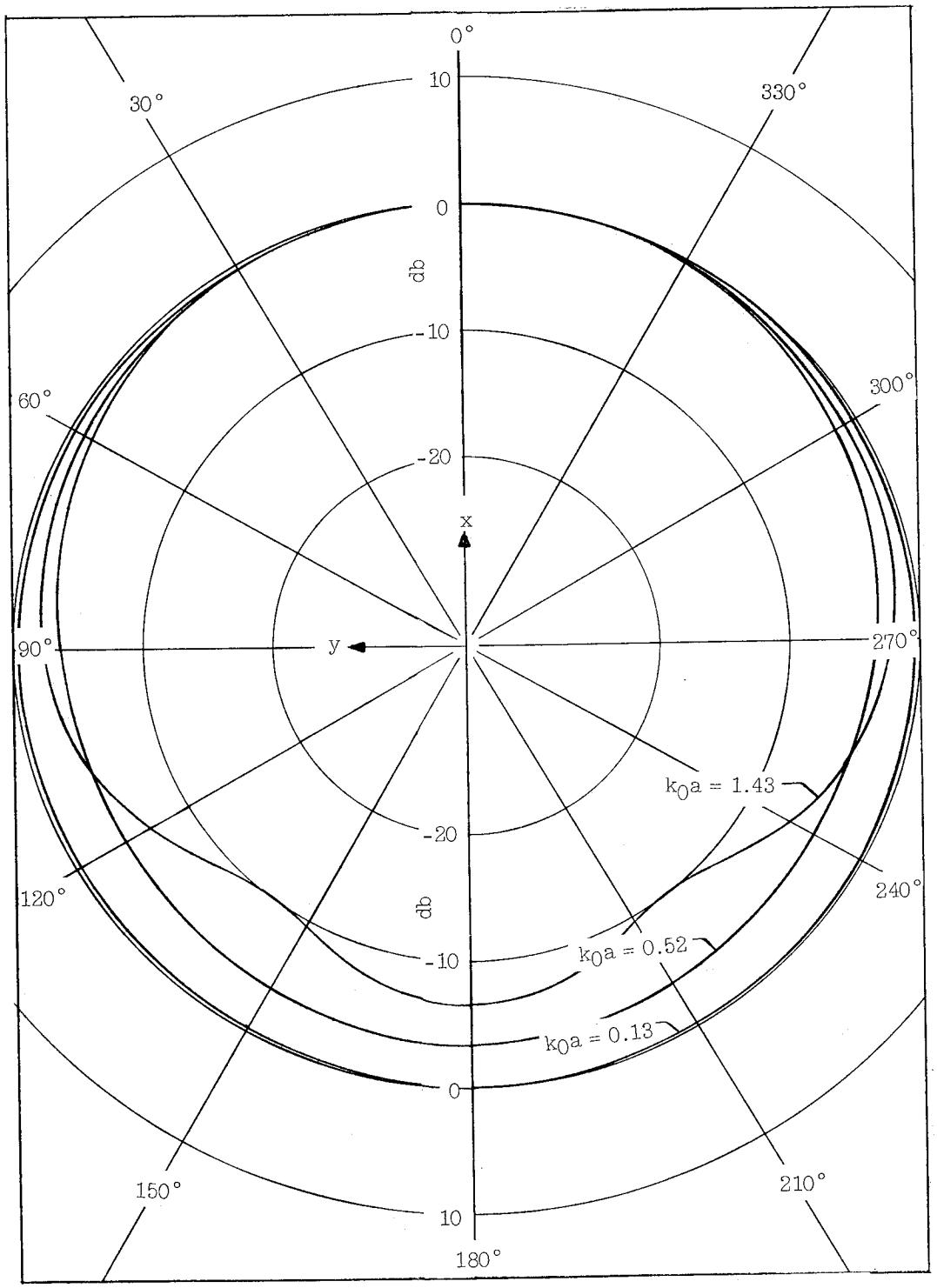

Figure 2.- Free-space patterns for k_0a = 0.13, 0.52, and 1.43.

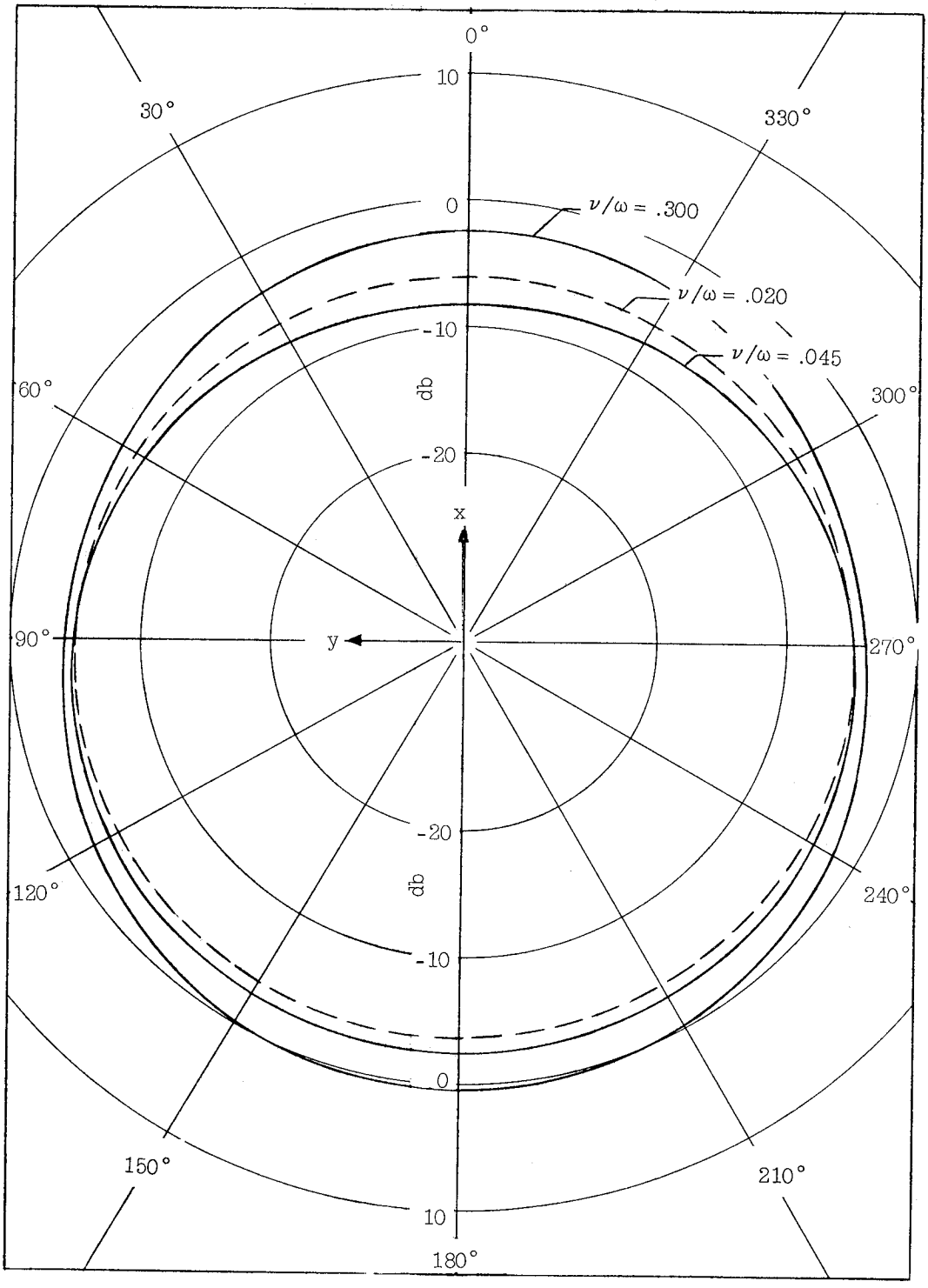

(a) $\omega/\omega_p = 1.0$.

Figure 3.- Effect of plasma frequency, collision frequency, coating thickness, and structure size on antenna patterns for $k_0a = 0.52$ and $b/a = 1.2$. Homogeneous plasma.

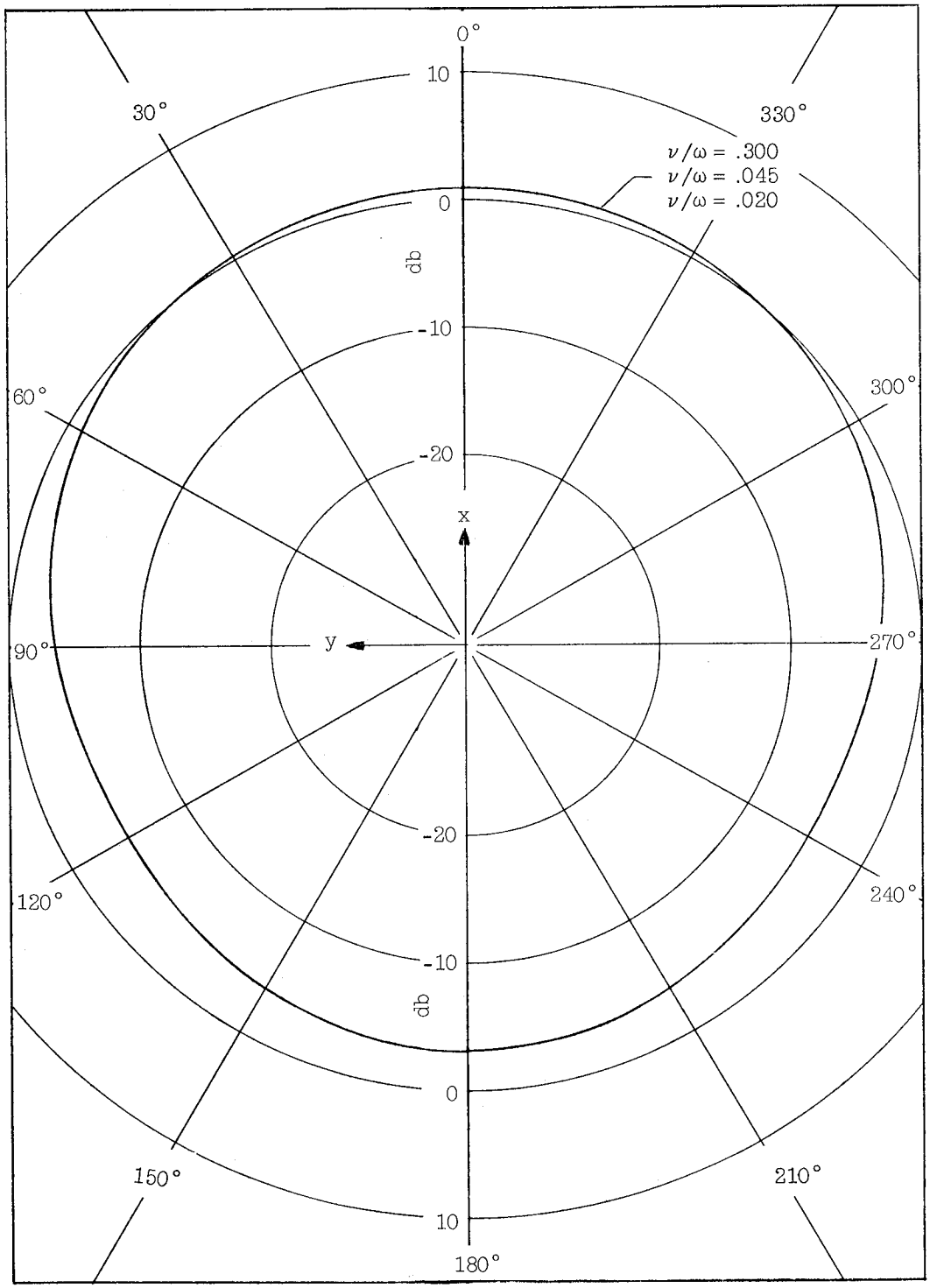

(b) $\omega/\omega_p = 0.30$.

Figure 3.- Continued.

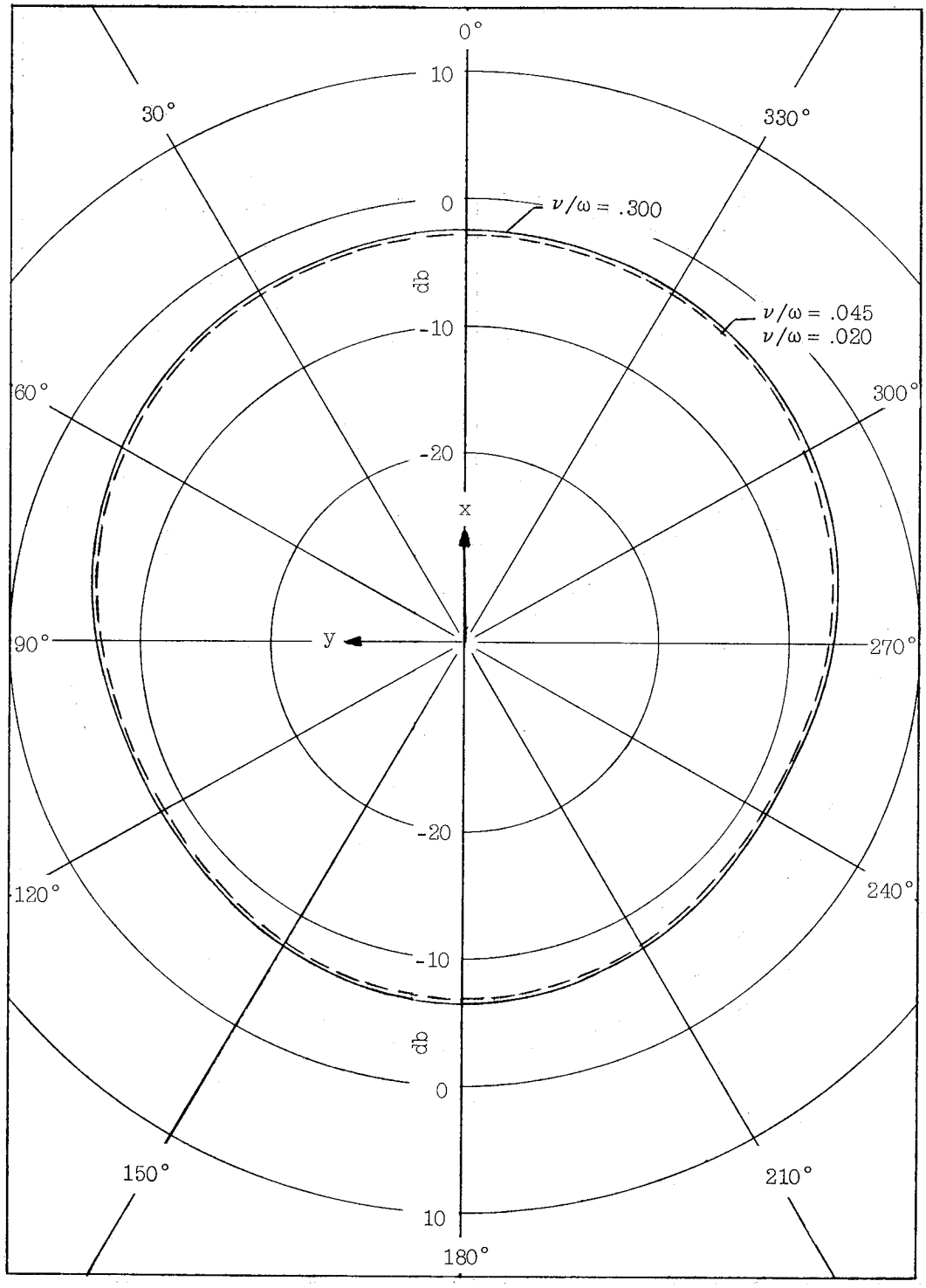

(c) $\omega/\omega_p = 0.10$.

Figure 3.- Continued.

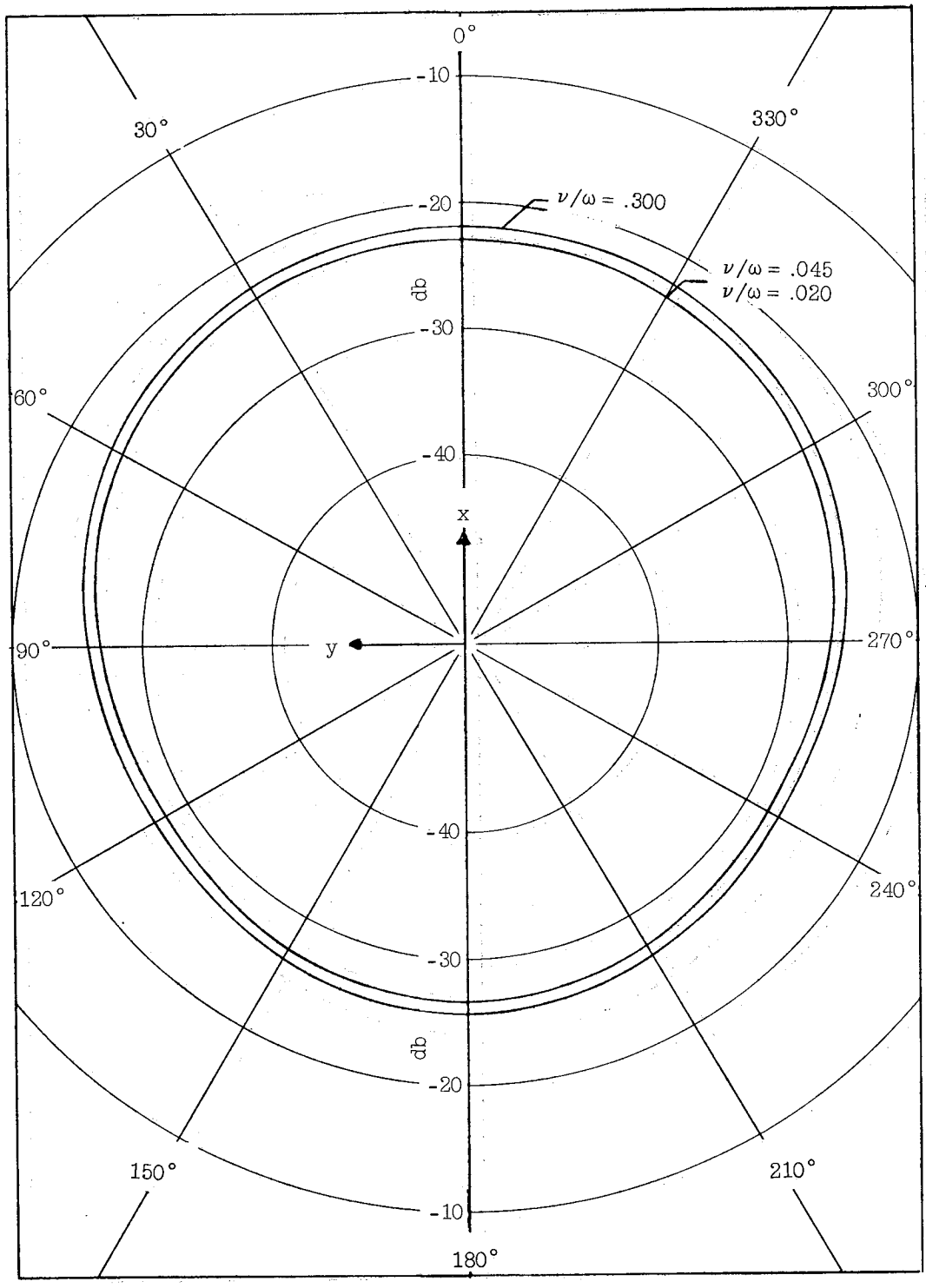

(d) $\omega/\omega_p = 0.03$.

Figure 3.- Continued.

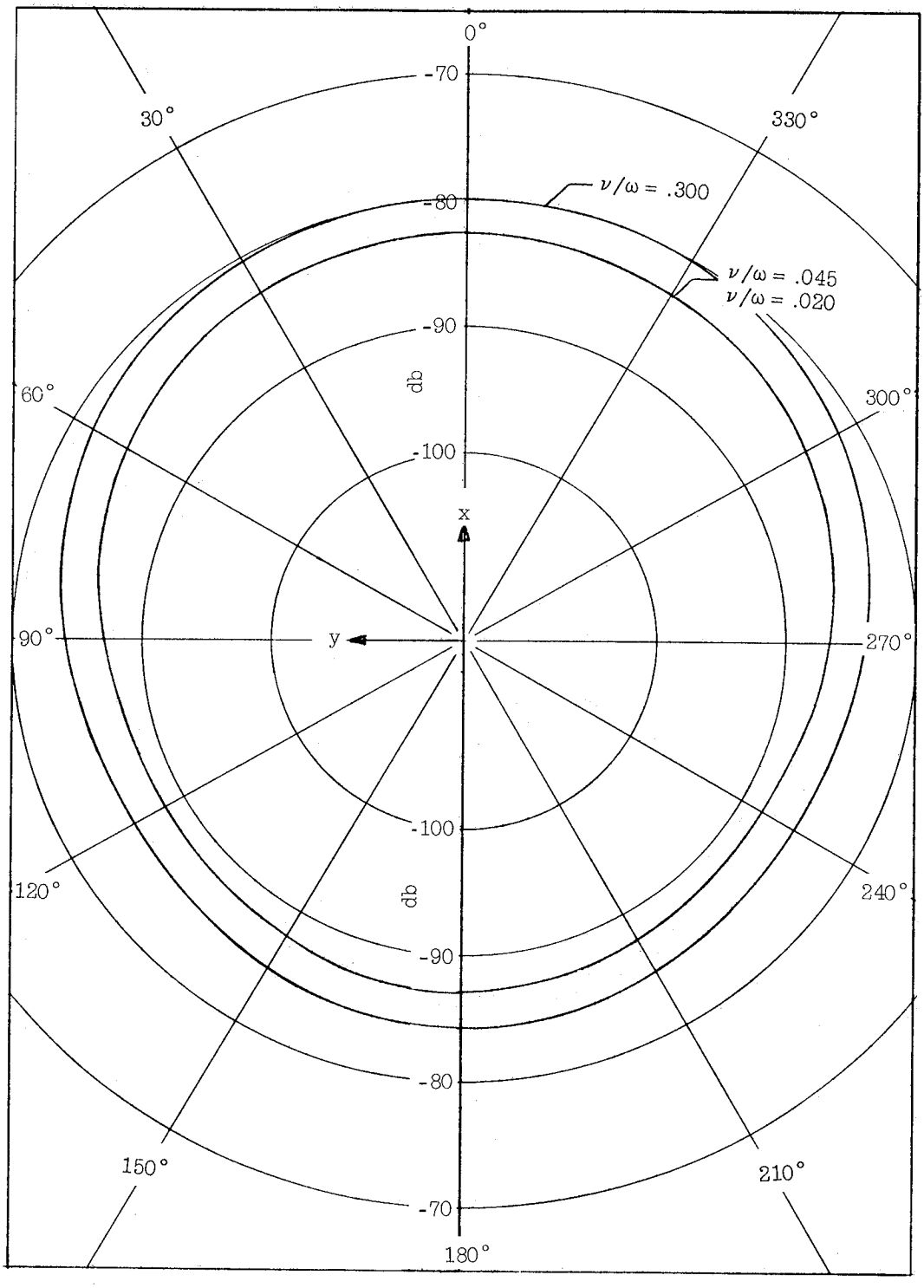

(e) $\omega/\omega_p = 0.01$.

Figure 3.- Concluded.

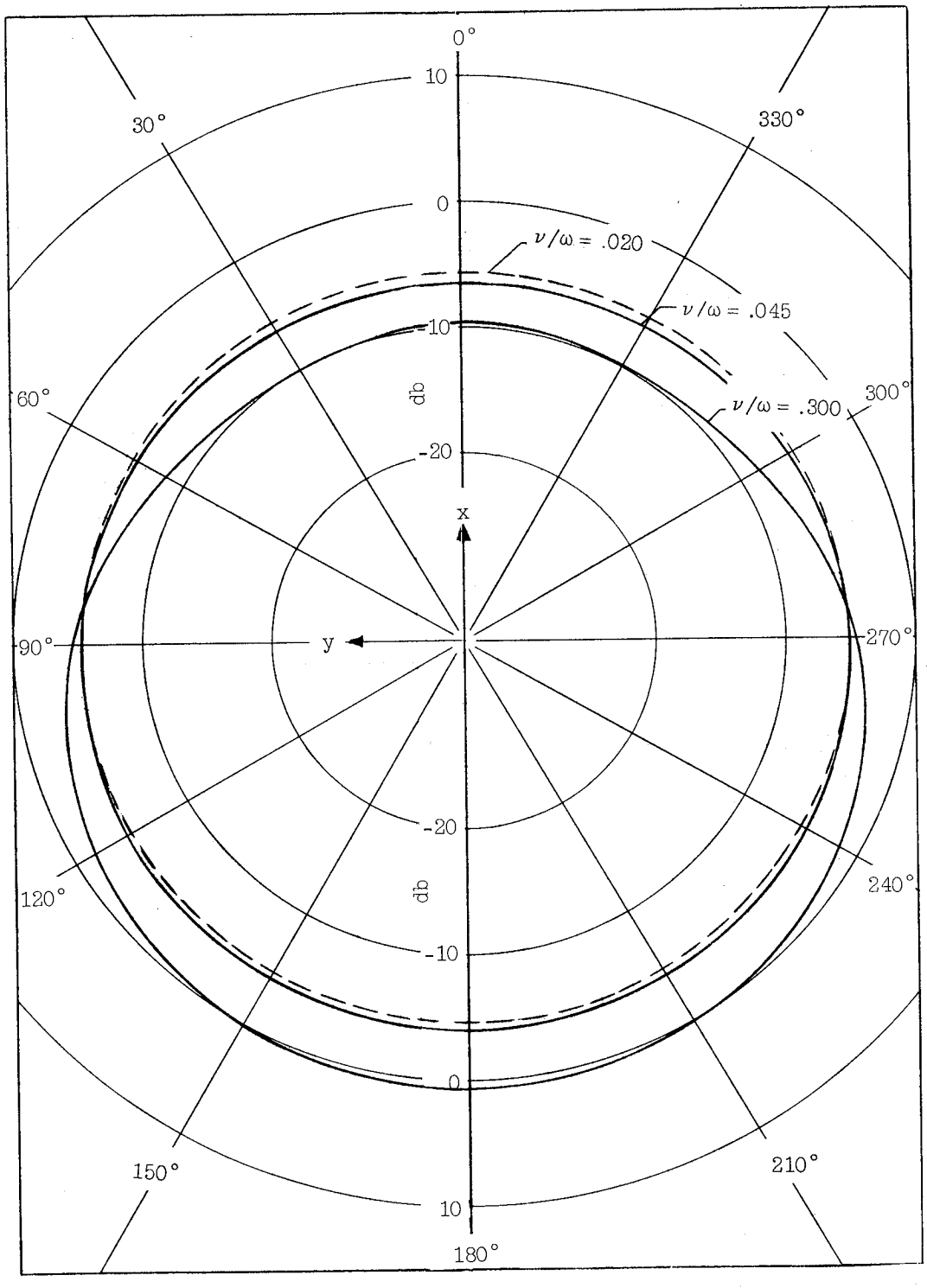

(a) $\omega/\omega_p = 1.0$.

Figure 4.- Effect of plasma frequency, collision frequency, coating thickness, and structure size on antenna patterns for $k_0a = 0.52$ and $b/a = 1.6$. Homogeneous plasma.

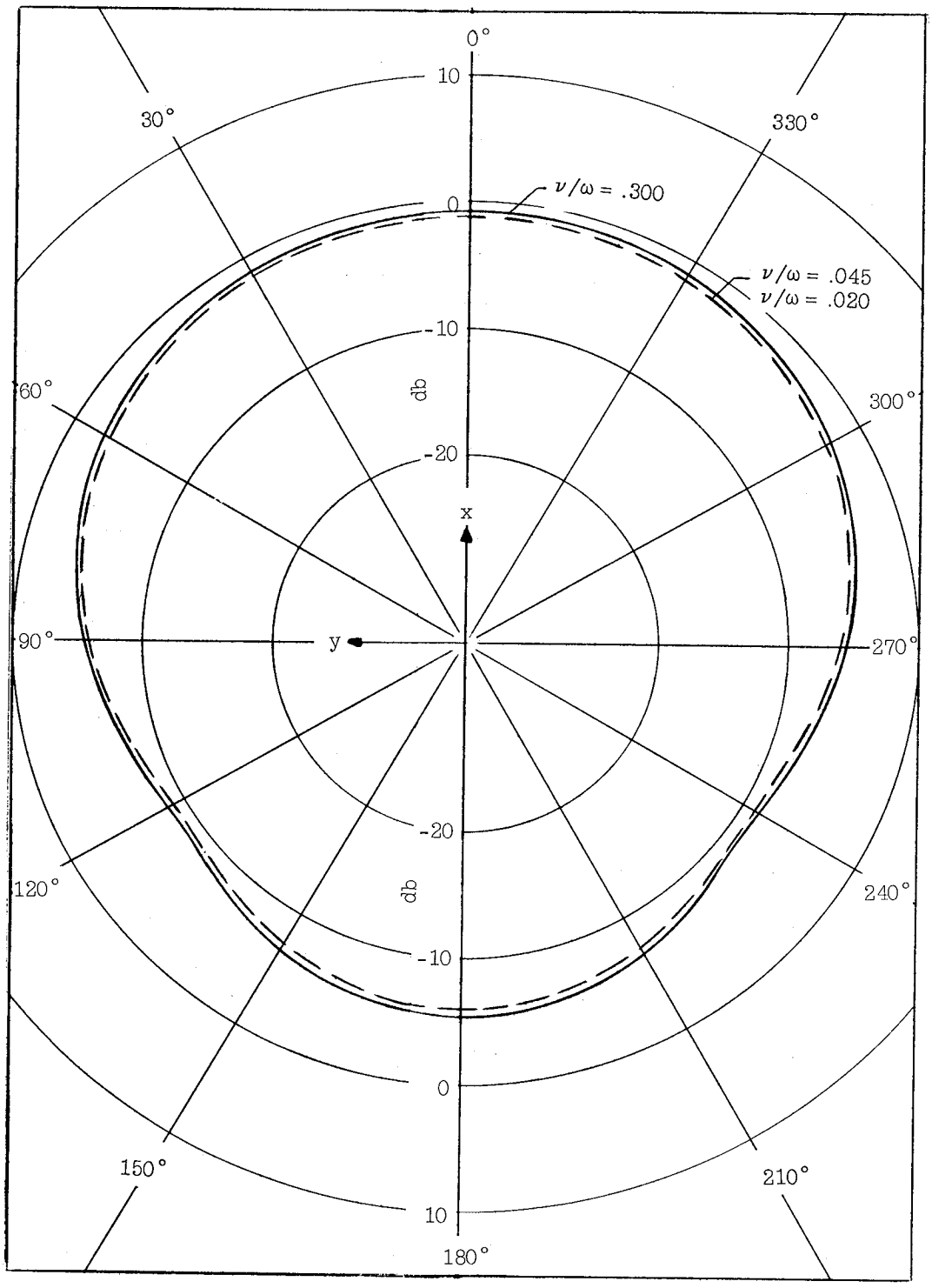

(b) $\omega/\omega_p = 0.30$.

Figure 4.- Continued.

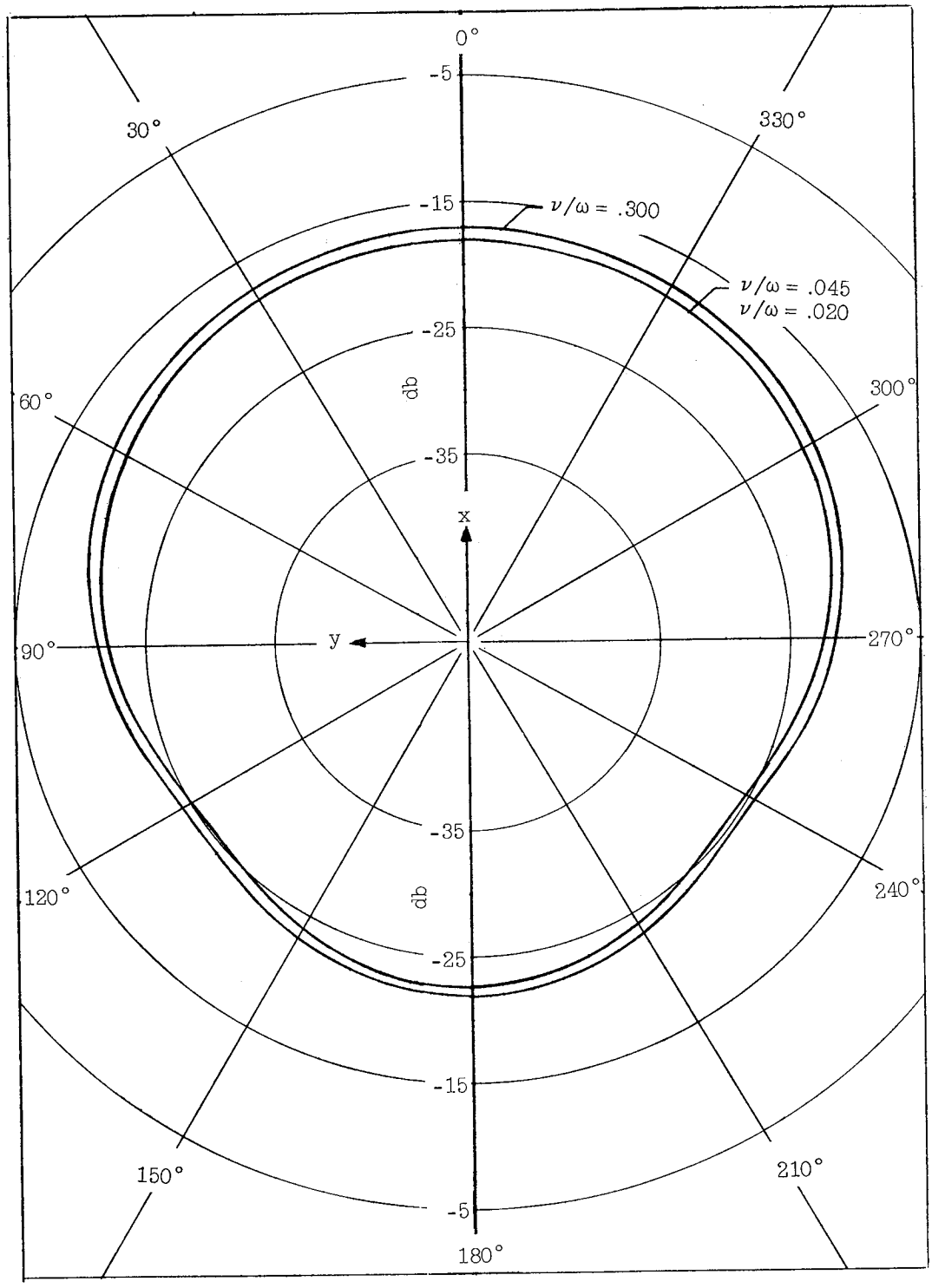

(c) $\omega/\omega_p = 0.10$.

Figure 4.- Continued.

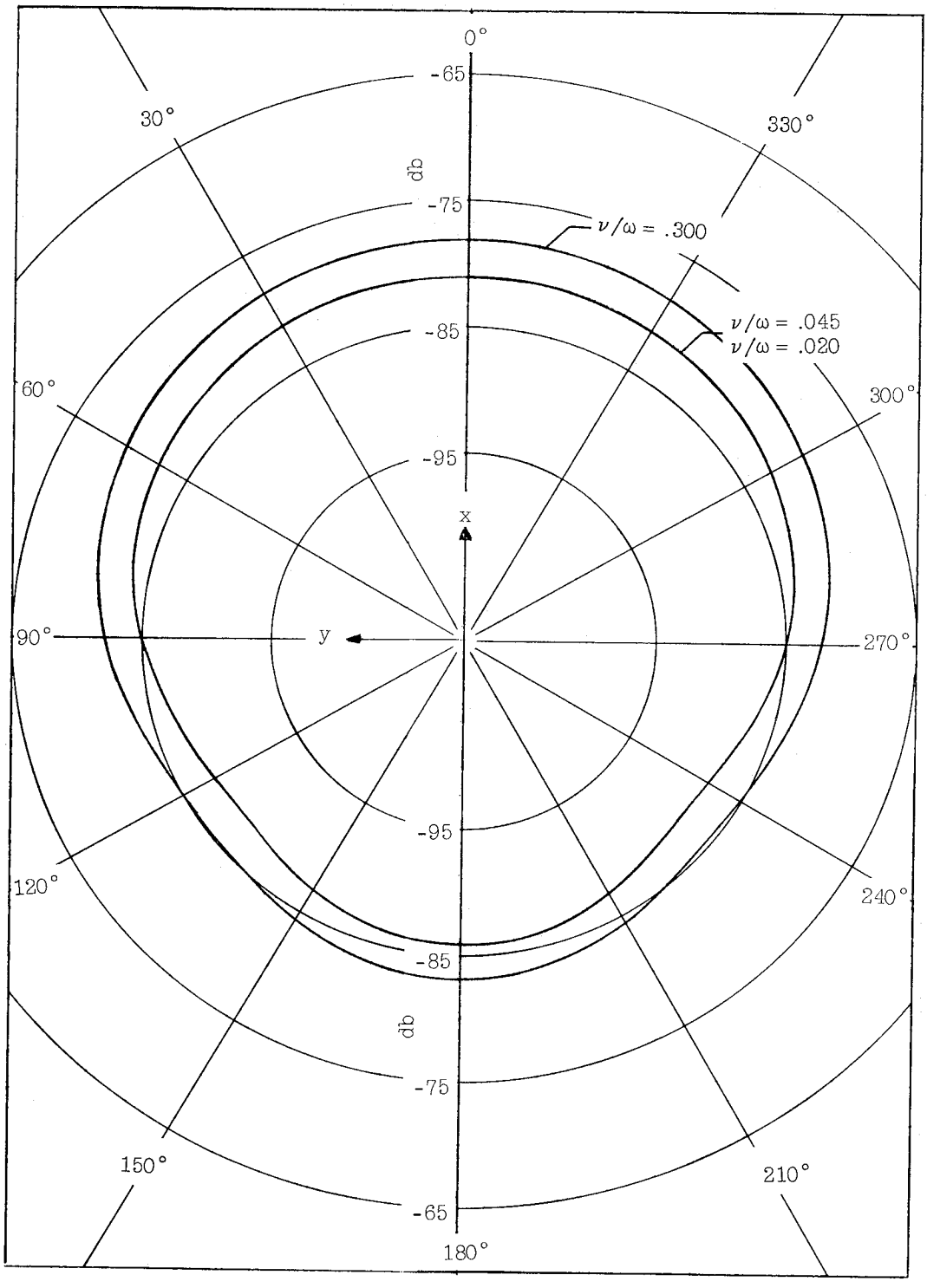

(d) $\omega/\omega_p = 0.03$.

Figure 4.- Concluded.

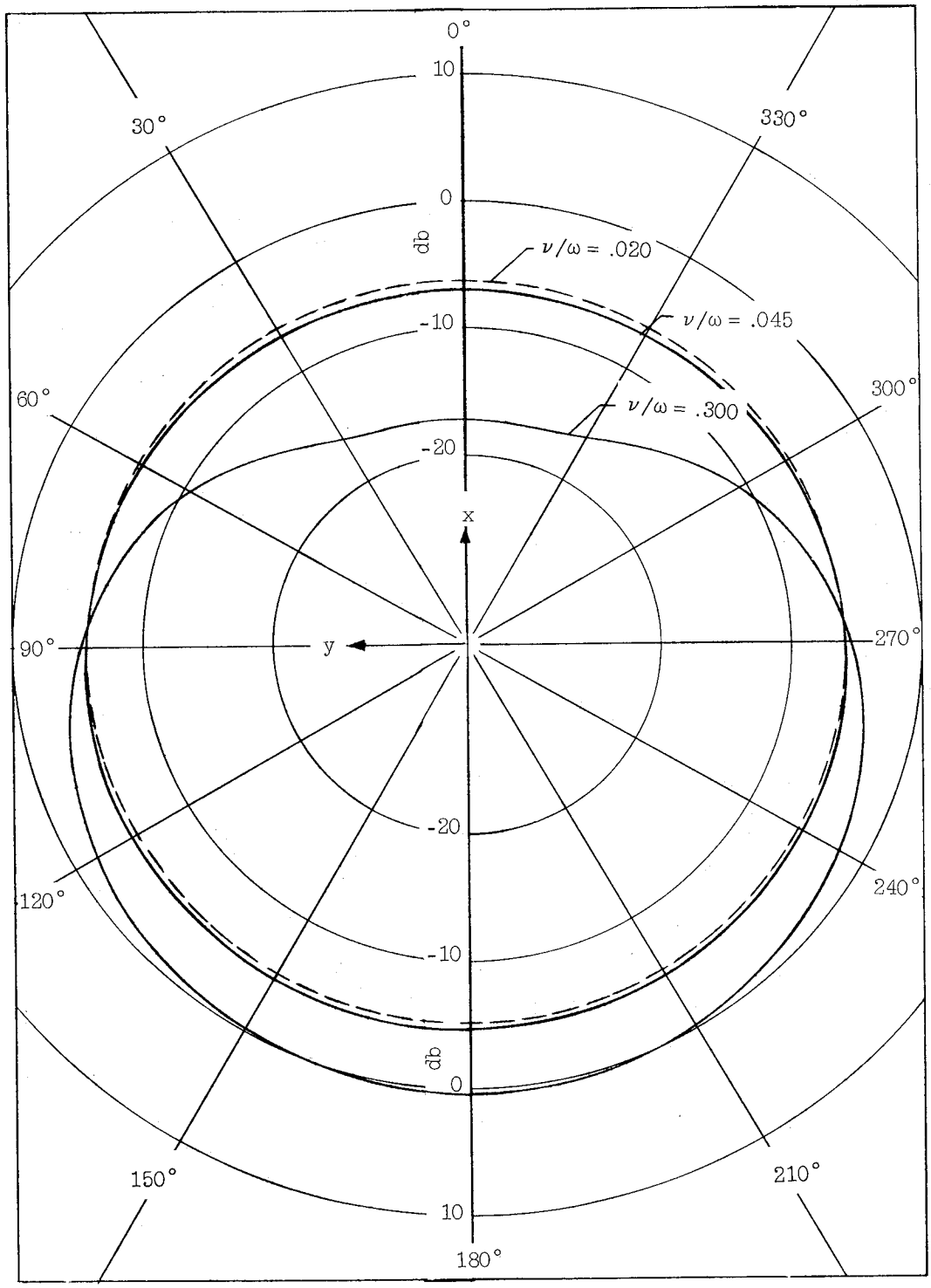

(a) $\omega/\omega_p = 1.0$.

Figure 5.- Effect of plasma frequency, collision frequency, coating thickness, and structure size on antenna patterns for $k_0a = 0.52$ and $b/a = 2.0$. Homogeneous plasma.

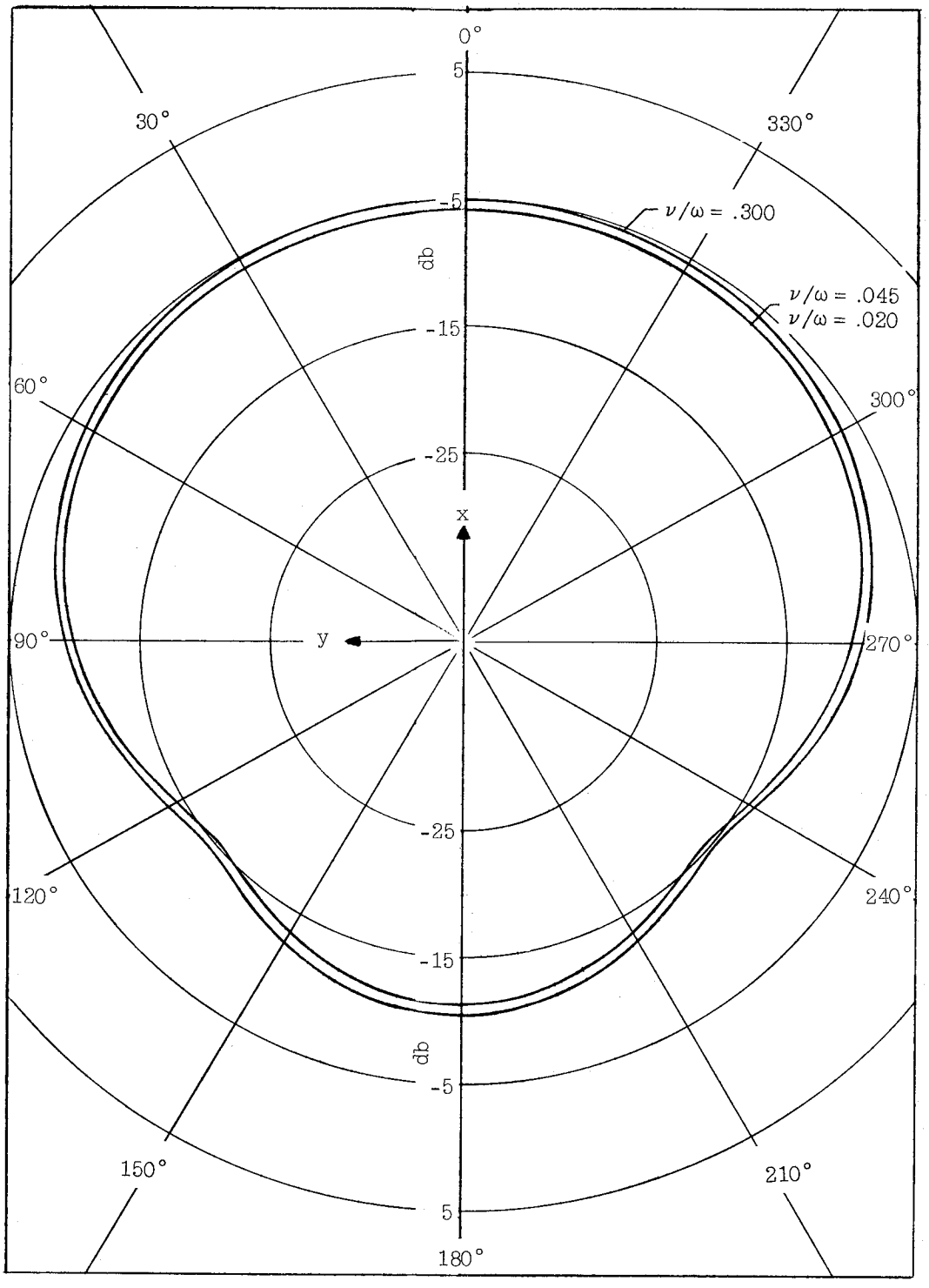

(b) ω/ω_p = 0.30.

Figure 5.- Continued.

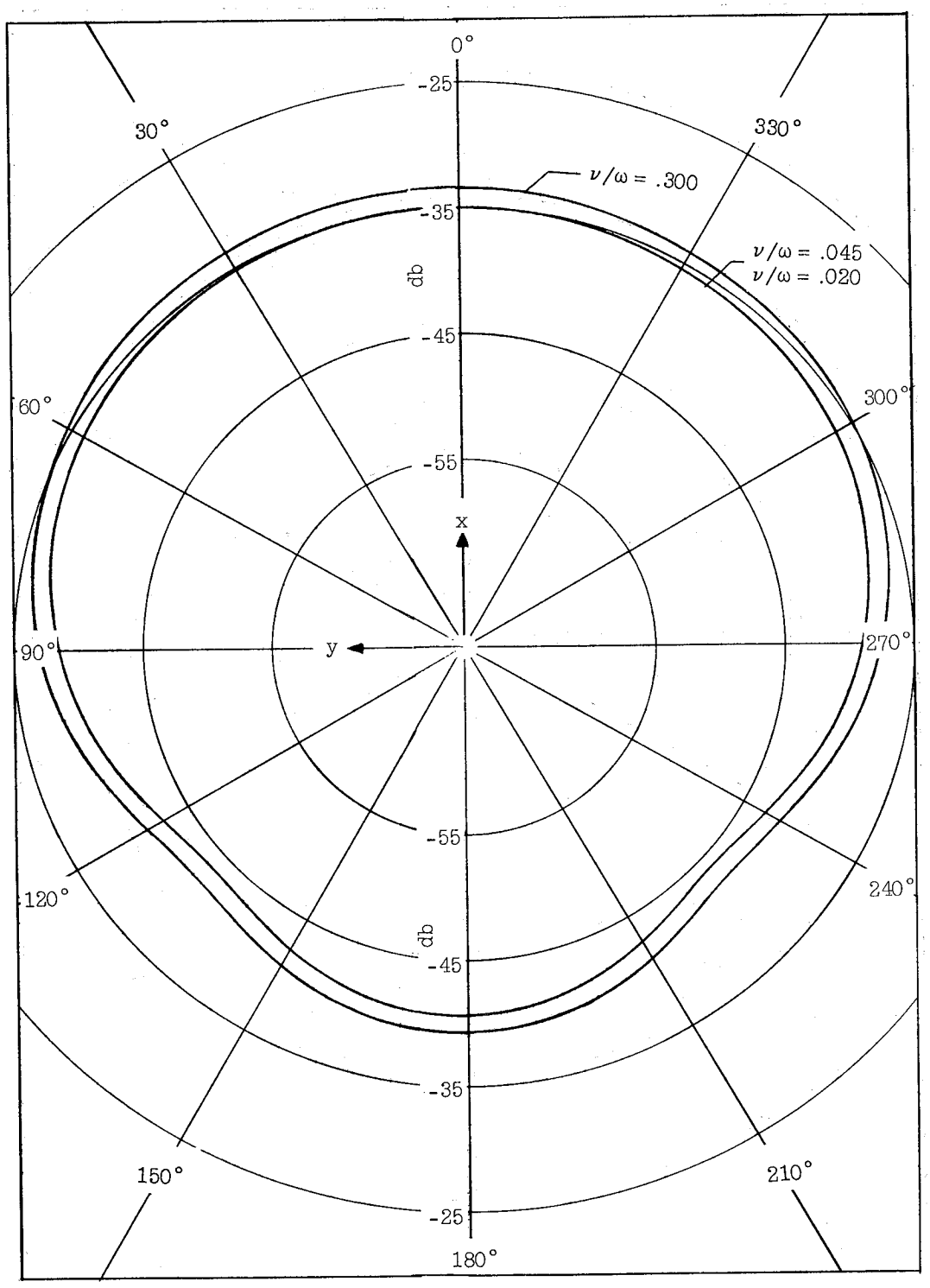

(c) $\omega/\omega_p = 0.10$.

Figure 5.- Concluded.

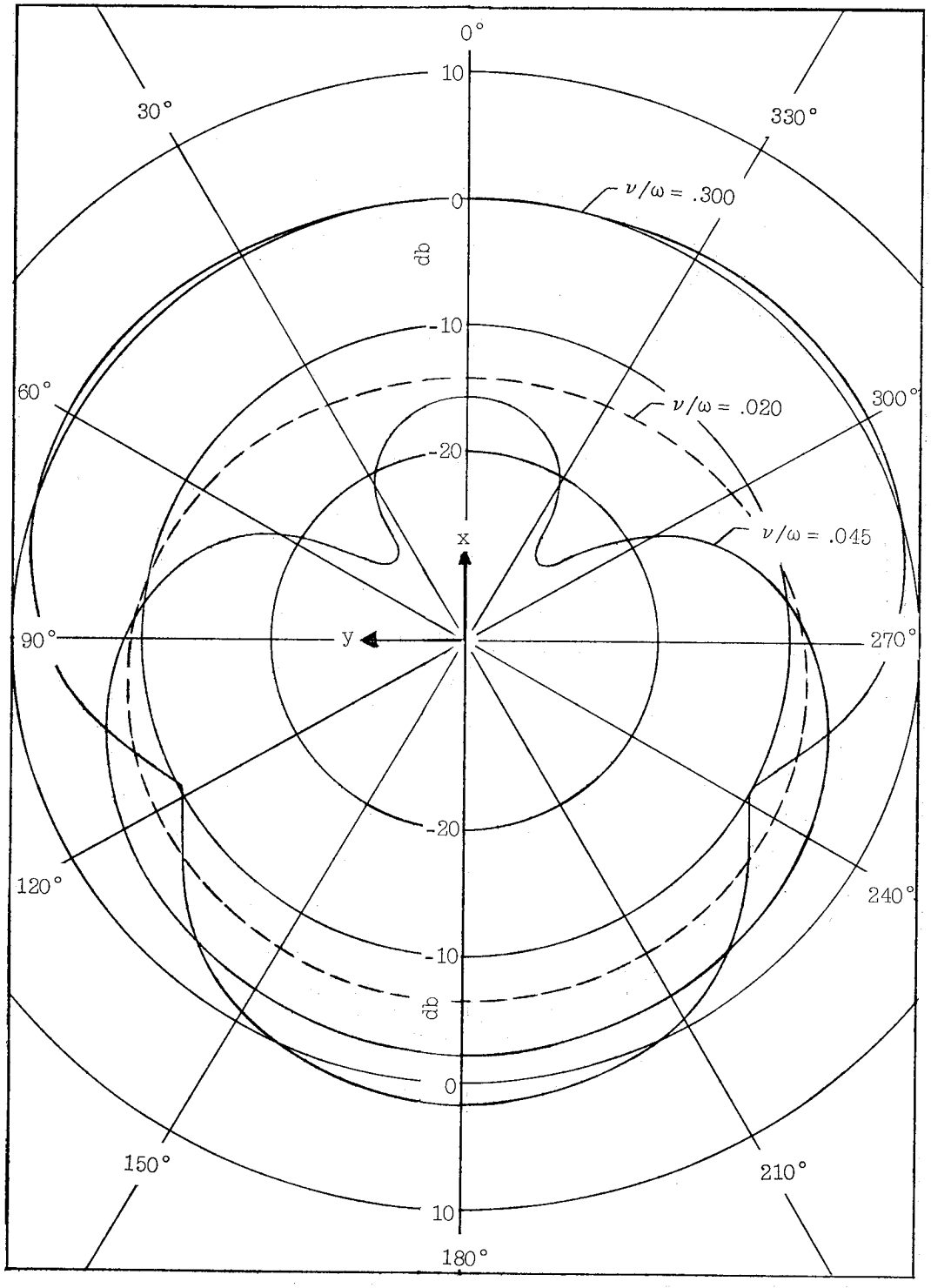

(a) $\omega/\omega_p = 1.0$.

Figure 6.- Effect of plasma frequency, collision frequency, coating thickness, and structure size on antenna patterns for $k_0a = 1.43$ and $b/a = 1.20$. Homogeneous plasma.

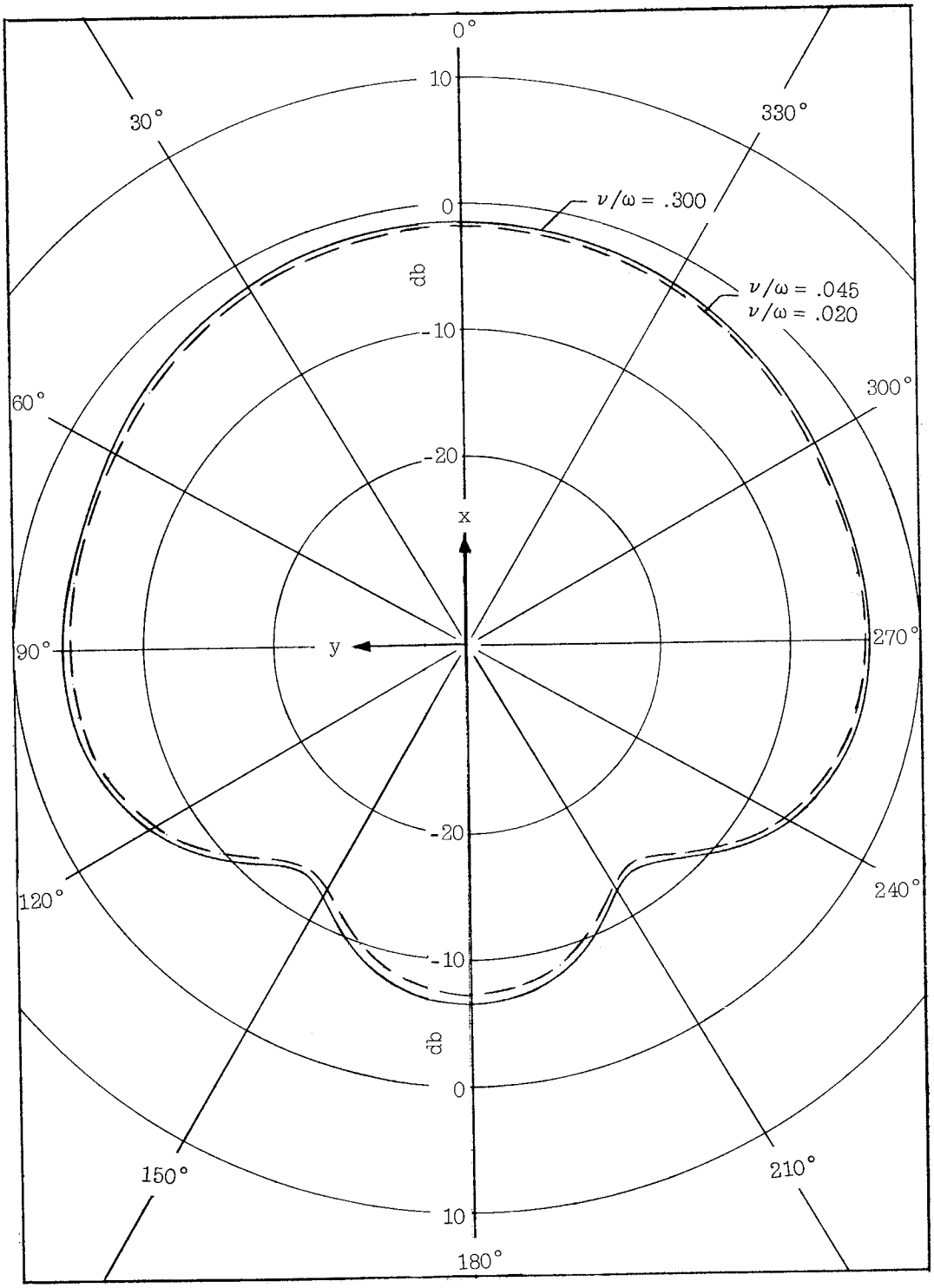

(b) $\omega/\omega_p = 0.30$.

Figure 6.- Continued.

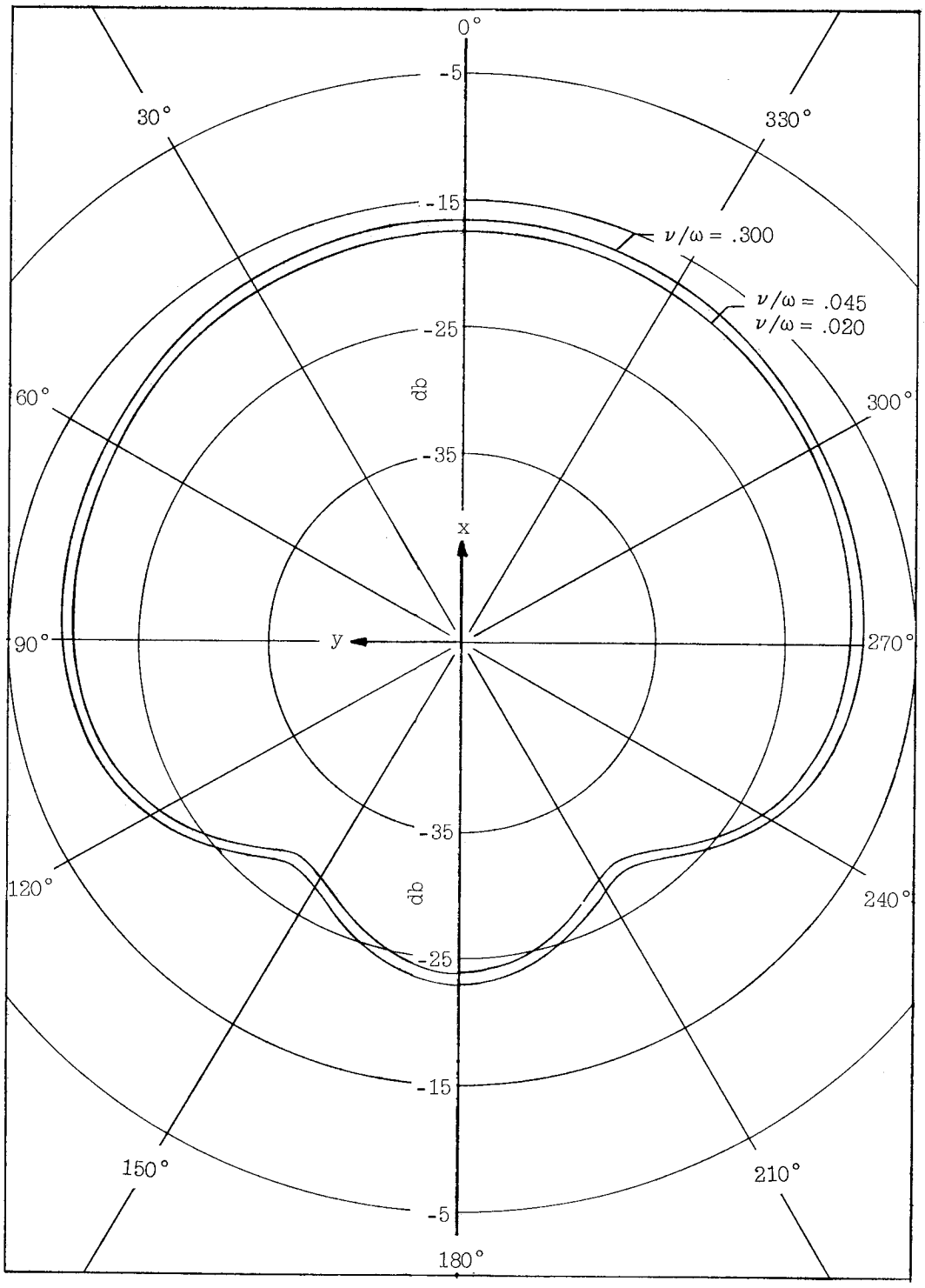

(c) $\omega/\omega_p = 0.10$.

Figure 6.- Continued.

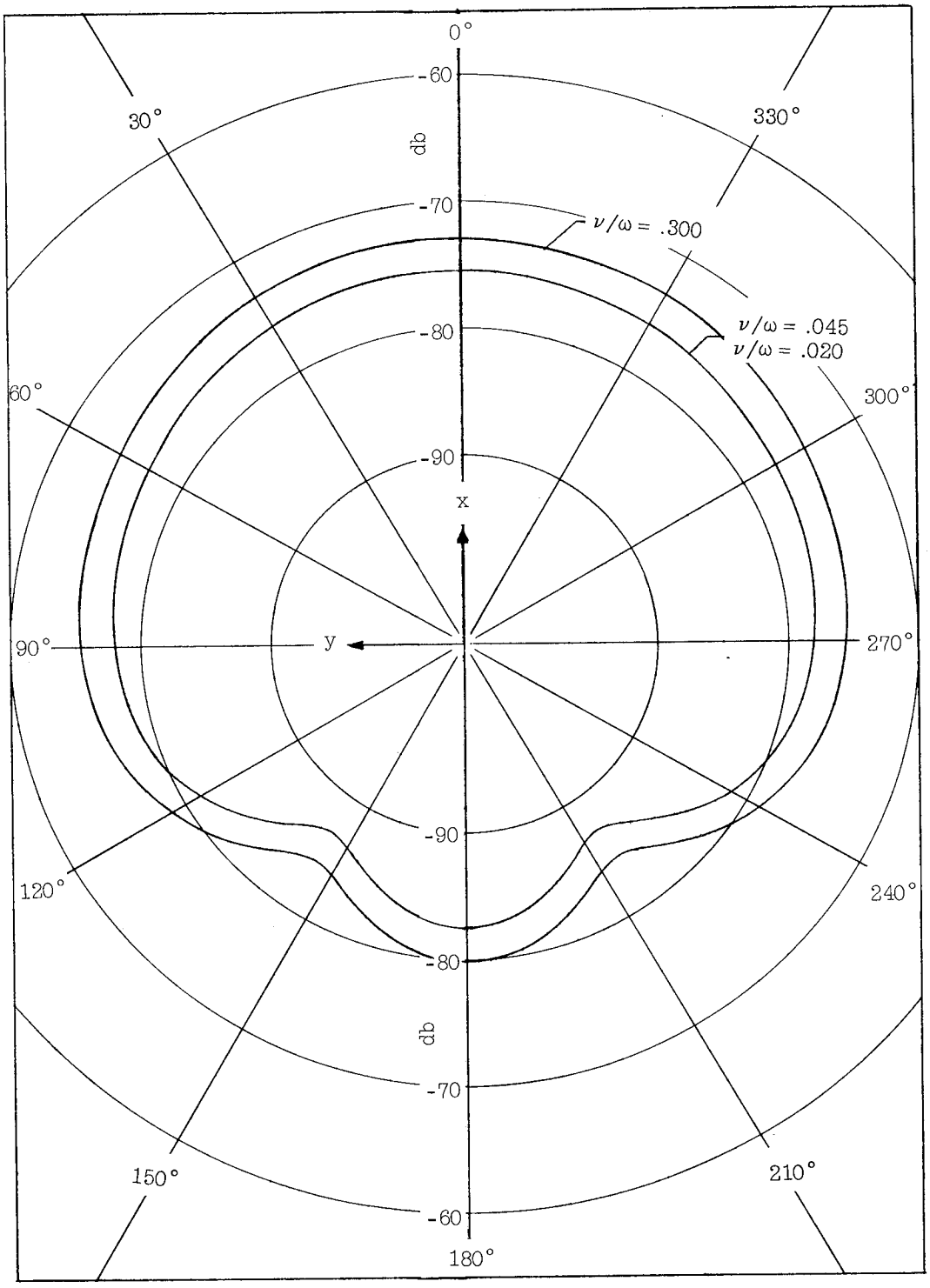

(d) $\omega/\omega_p = 0.03$.

Figure 6.- Concluded.

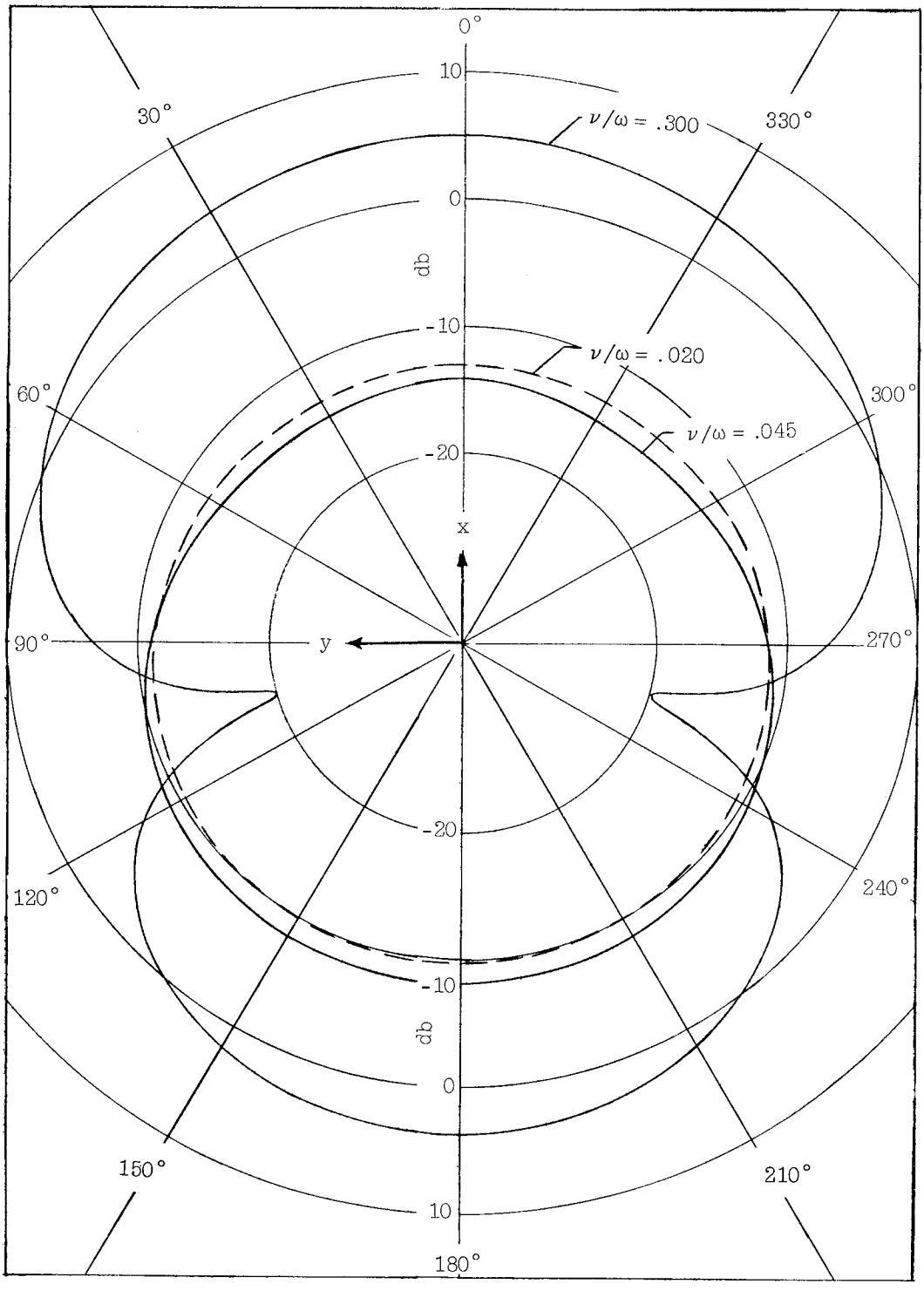

(a) $\omega/\omega_p = 1.0$.

Figure 7.- Effect of plasma frequency, collision frequency, coating thickness, and structure size on antenna patterns for $k_0a = 1.43$ and $b/a = 1.60$. Homogeneous plasma.

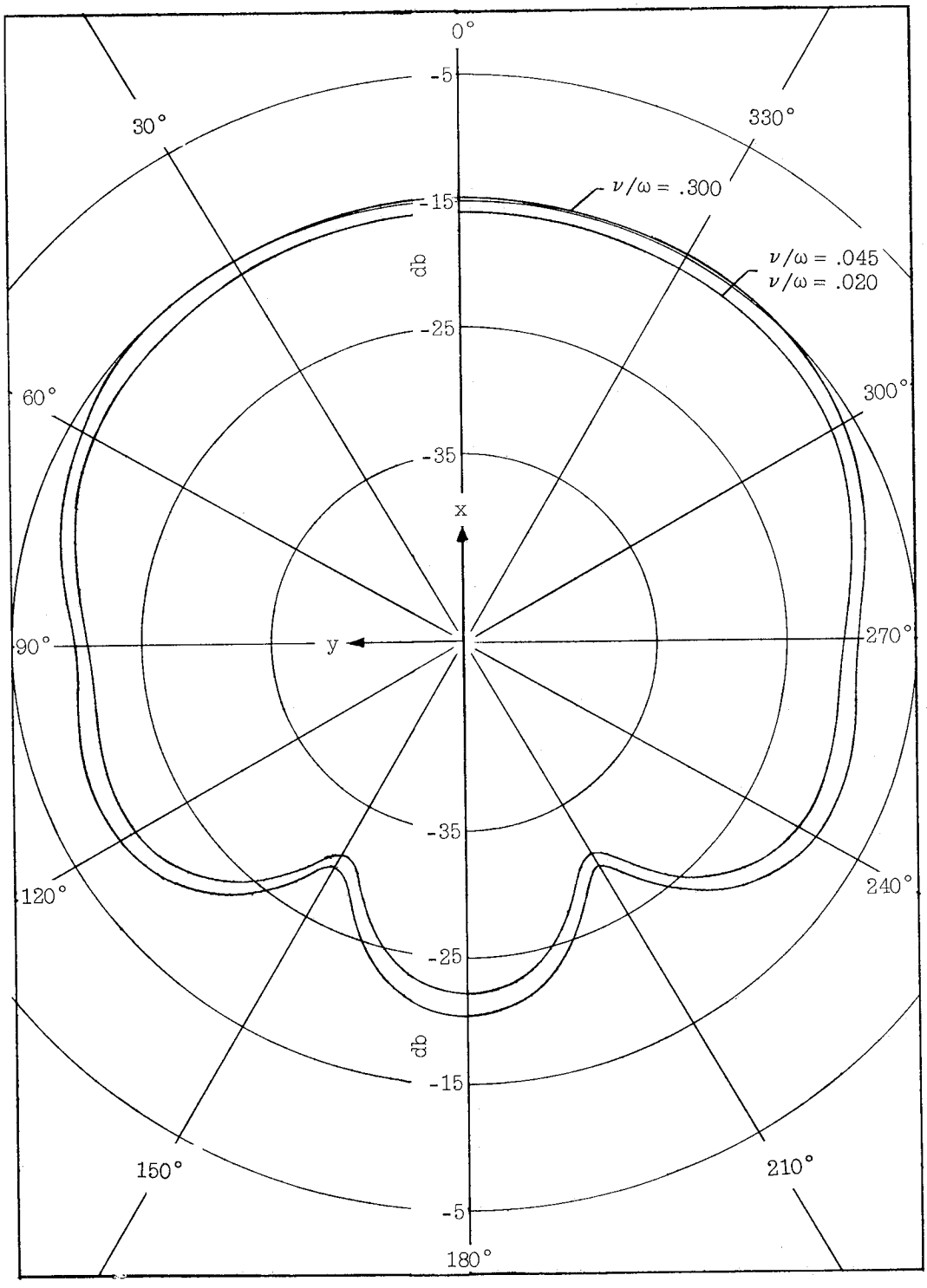

(b) $\omega/\omega_p = 0.30$.

Figure 7.- Continued.

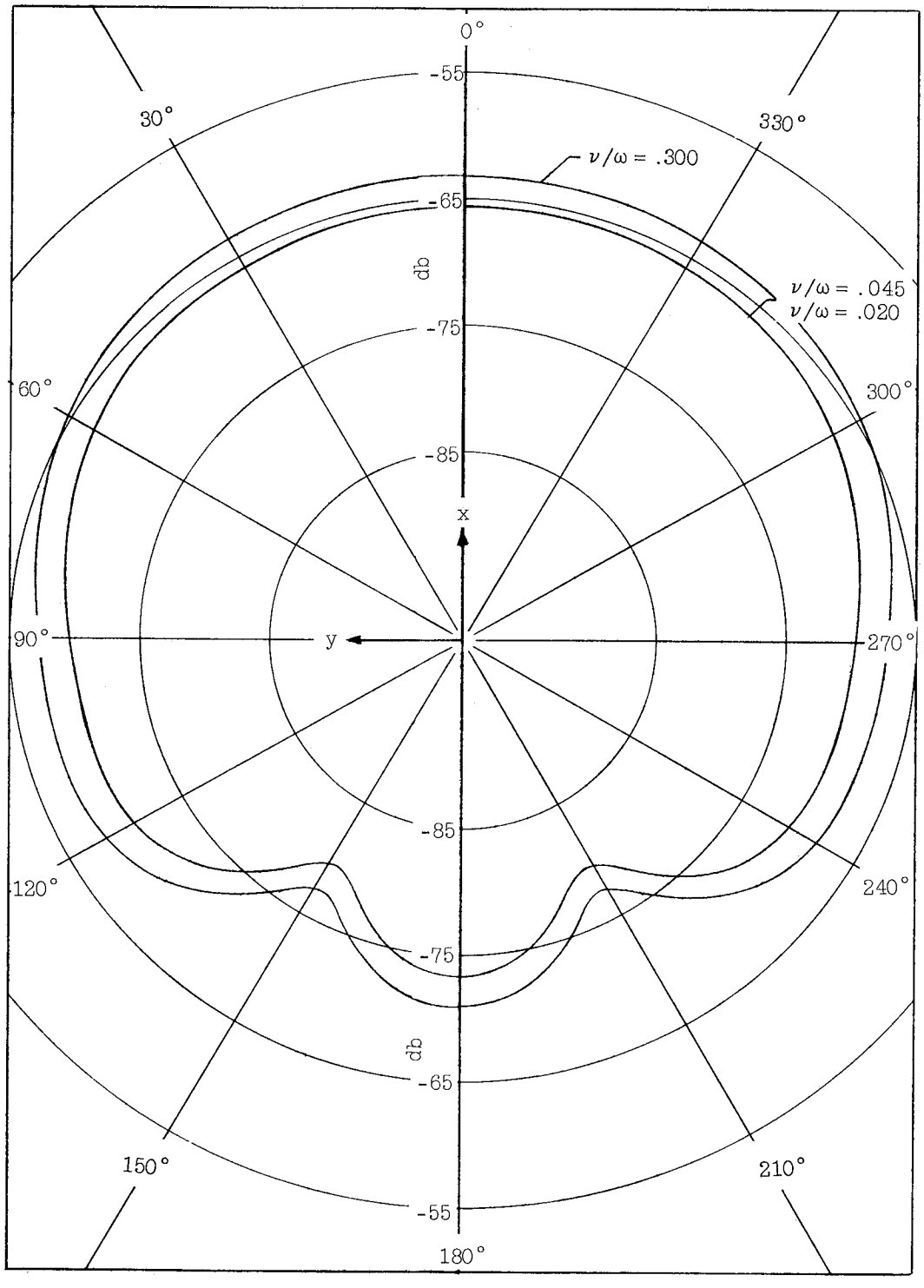

(c) $\omega/\omega_p = 0.10$.

Figure 7.- Concluded.

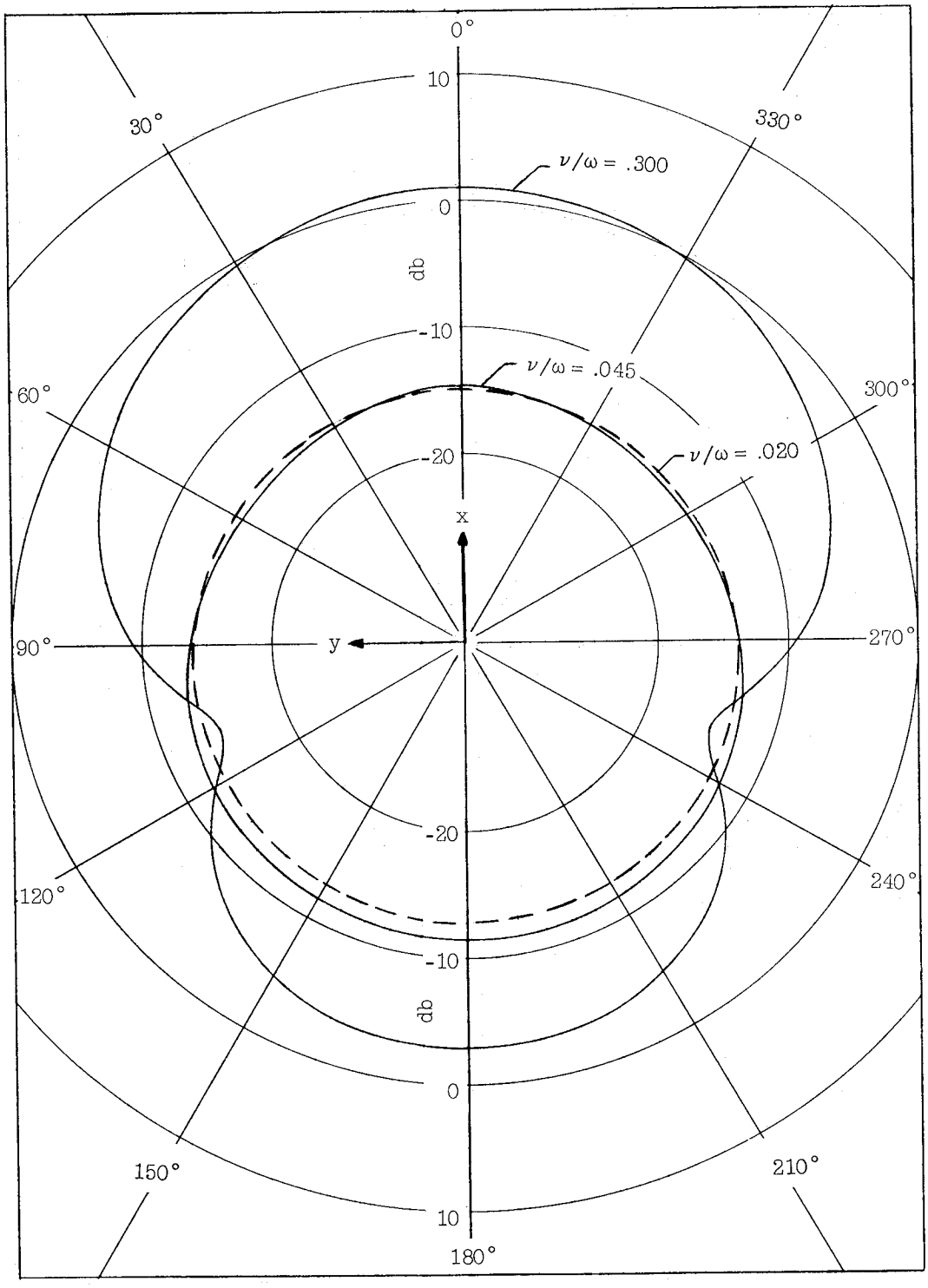

(a) $\omega/\omega_p = 1.0$.

Figure 8.- Effect of plasma frequency, collision frequency, coating thickness, and structure size on antenna patterns for $k_0a = 1.43$ and $b/a = 2.0$.

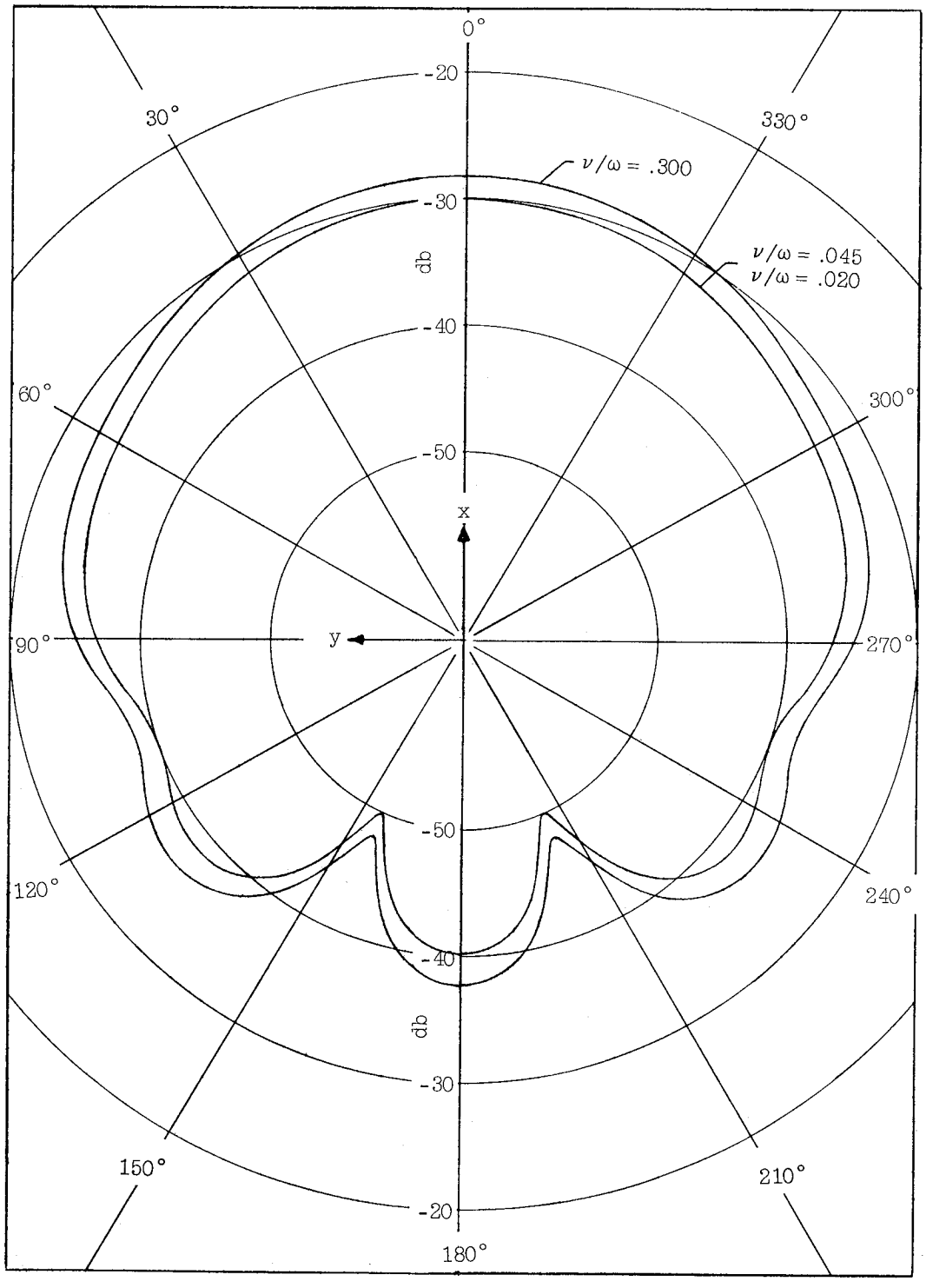

(b) $\omega/\omega_p = 0.30$.

Figure 8.- Concluded.

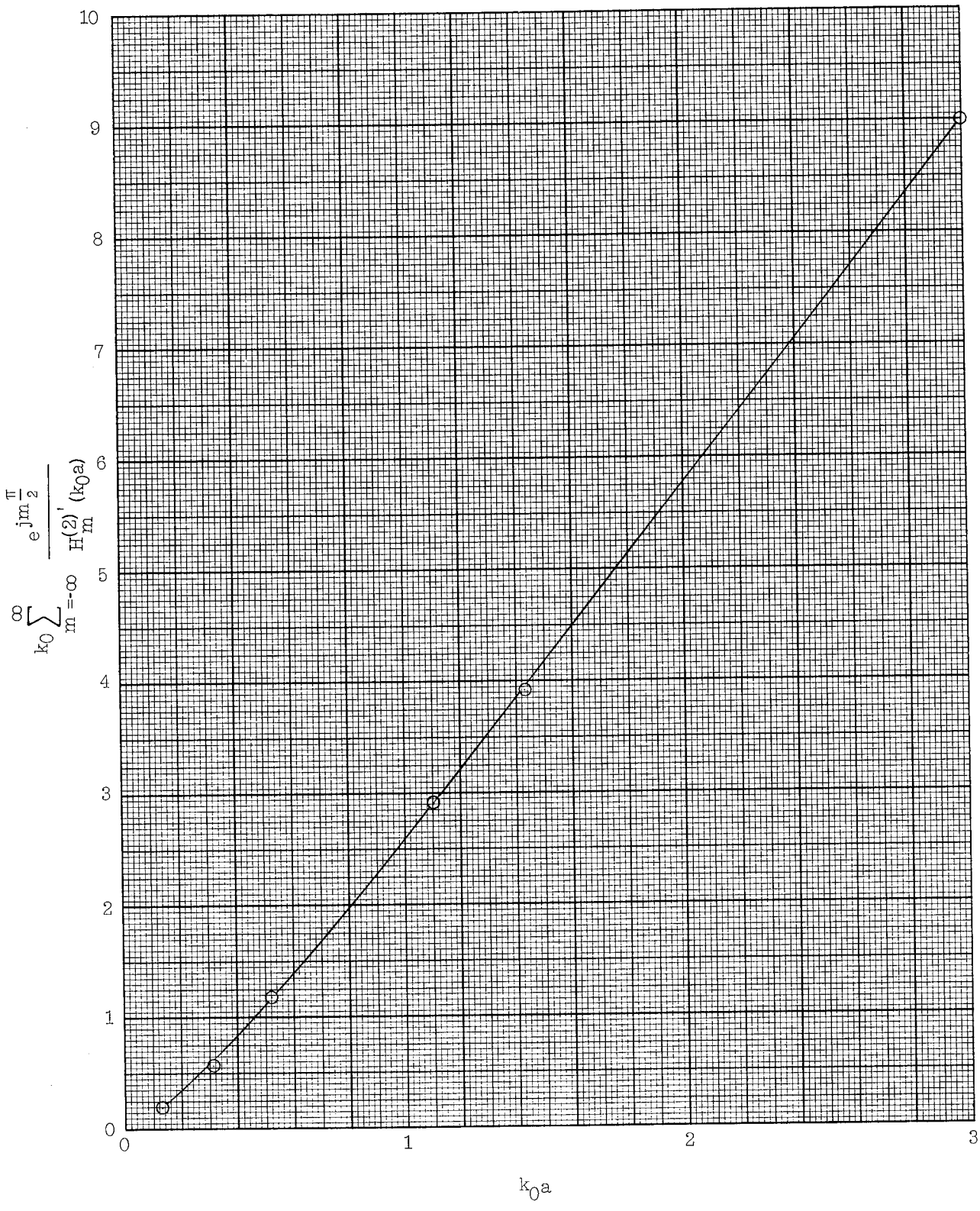

Figure 9.- Pattern strength at $\phi = 0^\circ$ for an uncoated cylinder as a function of $k_0 a$.

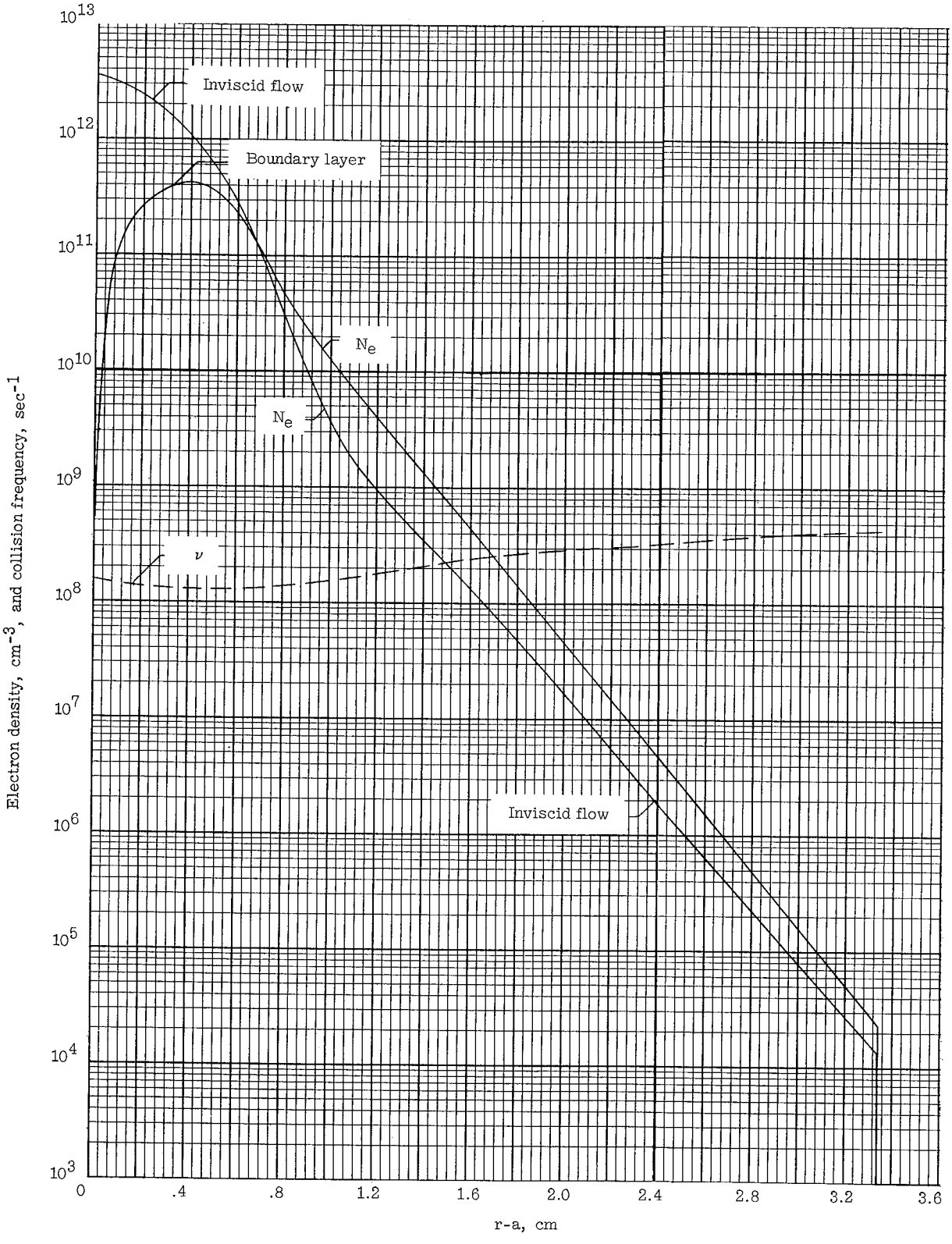

Figure 10.- Electron density and collision frequency distributions in a shock layer.

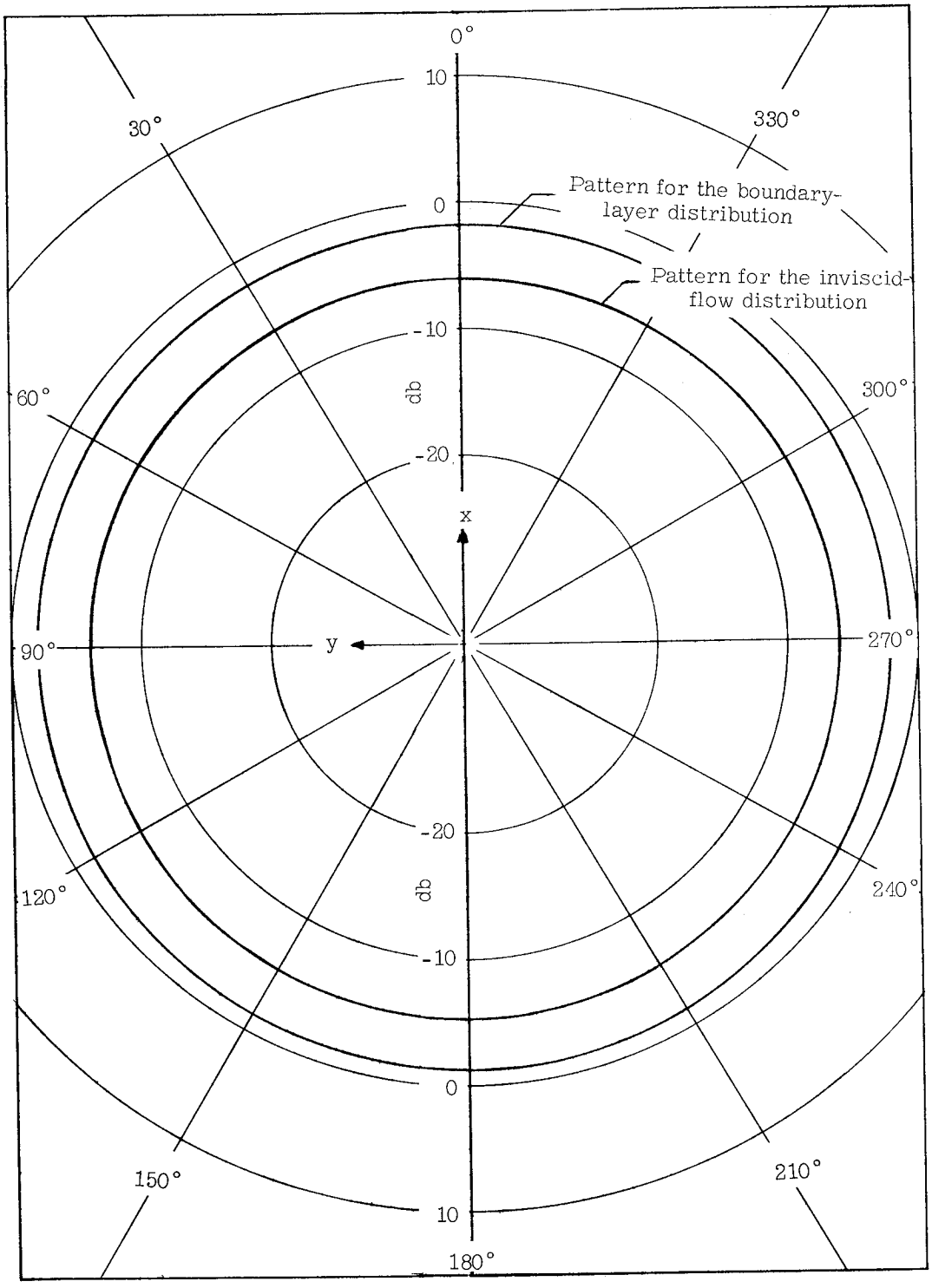

Figure 11.- Antenna patterns resulting from the distributions given in figure 10. Frequency, 244.3 mc; $k_0a = 0.13$.

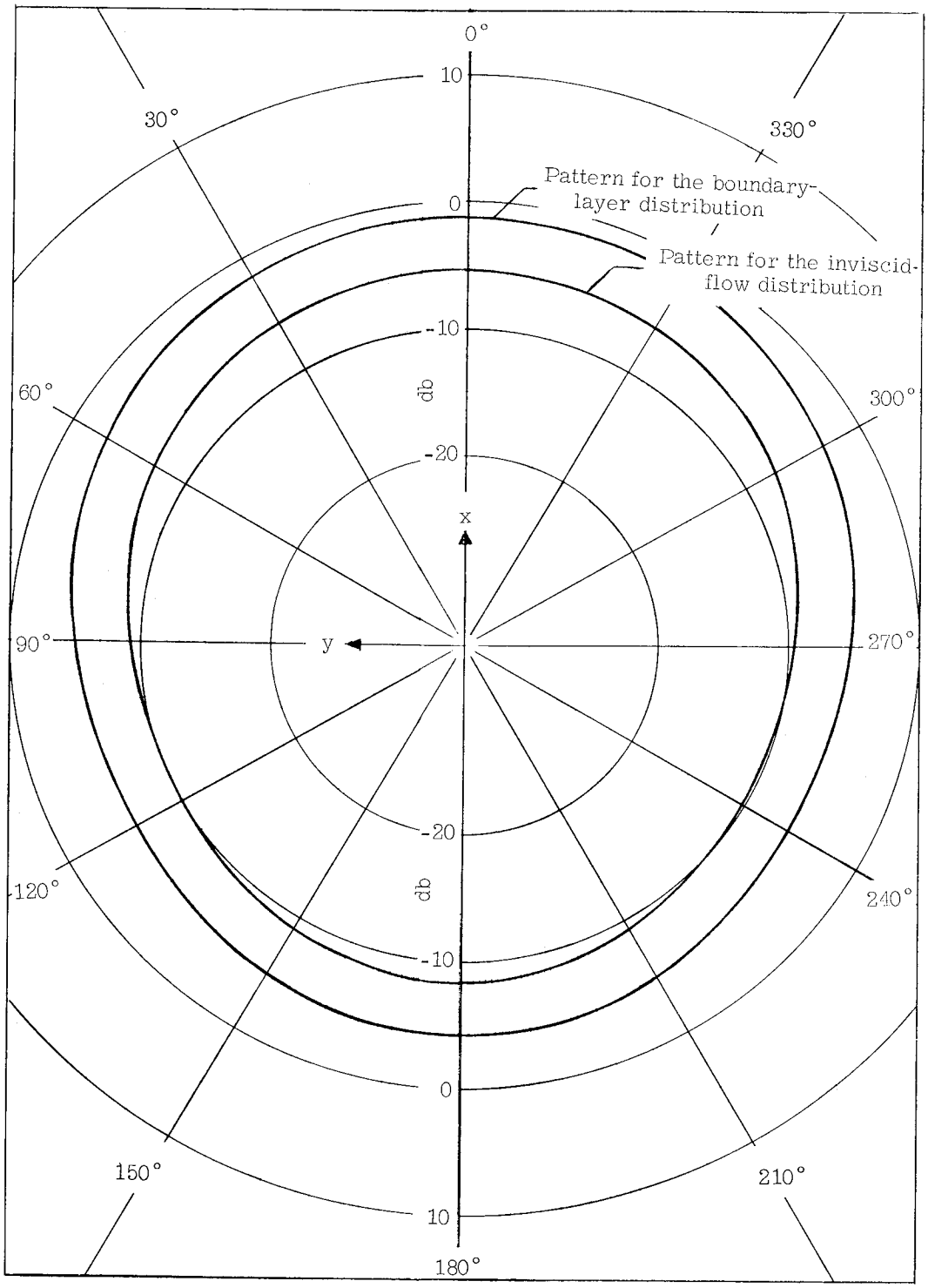

Figure 12.- Antenna patterns resulting from the distributions given in figure 10. Frequency, 244.3 mc; $k_0a = 0.52$.

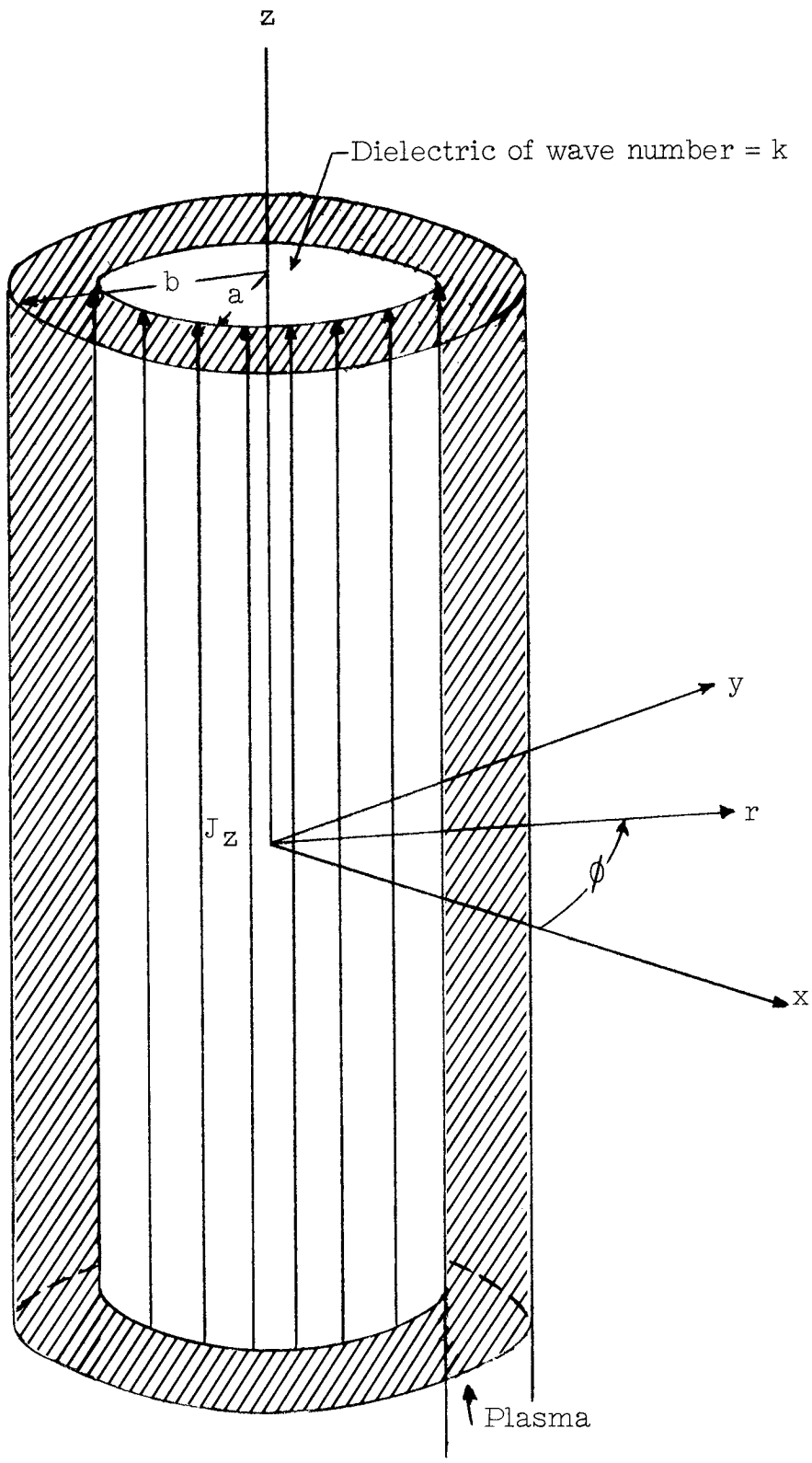

Figure 13.- Geometry of a cylinder of currents.